Chapter 5
Direct Reactions at Relativistic Energies: A New Insight into the Single-Particle Structure of Exotic Nuclei

Dolores Cortina-Gil

5.1 Introduction

Direct reactions are an excellent tool for the investigation of nuclear structure. They proceed in a single step and are very fast, $\approx 10^{-22}$ s, taking simply the time needed for the projectile to traverse a target nucleus. Usually, only a few bodies (nucleons) participate in the reaction. Moreover, only a few degrees of freedoms are involved and the momentum transfer associated is not very high. They are thus rather peripheral interactions mostly surface dominated. All these properties make the reaction mechanism easier to interpret and allow the use of a certain number of simplifications in their description. The high selectivity associated with direct reactions is also responsible for the dominance of single-particle properties over dynamical effects, opening the possibility of using them as spectroscopic tools.

The spectra of possible direct reactions is rather large and includes, among others, processes related to elastic, inelastic, transfer and knockout reactions. The use of direct reactions was vigorously extended throughout the 60–80 s with the advent of the first accelerators dedicated to the study of stable isotopes. In the 90's, the availability of exotic beams heralded a new golden age with the extension of structural studies to these new rare species. On top of the relative simplicity, the reaction cross-section is rather large, allowing their use since the first beam deployment despite the rather low intensities of these radioactive beams.

Secondary beams at different energy regimes became widespread across several experimental facilities all over the world. Elastic and inelastic reactions induced by secondary exotic projectiles took hold as a powerful tool to gain information on the radius and matter densities associated with those exotic species.

These first experiments lead to others, more specific, that addressed the study of structural properties. Low energy facilities concentrated on the study of transfer reactions, able to provide detailed information on the single-particle properties

D. Cortina-Gil (✉)
Universidad de Santiago de Compostela, 15782 Santiago de Compostela, Spain
e-mail: d.cortina@usc.es

C. Scheidenberger, M. Pfützner (eds.), *The Euroschool on Exotic Beams, Vol. IV*, Lecture Notes in Physics 879, DOI 10.1007/978-3-642-45141-6_5,

of the different states connected with the reaction (see chapter by Joaquín Gómez Camacho and Antonio Moro in this volume for further information on this topic).

In addition, the exploration of removal reactions became very popular among the high energy facilities. These reactions are the result of the interaction between a fast projectile and a target at rest. The nature of the projectile-target interaction can be nuclear (light target) or Coulomb (heavy target). For large impact parameters, the reaction would be peripheral, and would result in the dissociation or breakup of the projectile into one or a few nucleons (neutrons or protons) that would be ejected and a quasi-projectile (very often called core-fragment) that would continue on its path largely unaffected by the reaction, with almost the same velocity as the incident projectile. Experimentally, the selection of the reaction channel is achieved by detecting the incident projectile and the emerging fragments (with mass *A-1* in the one nucleon-removal case). The survival of the fragment is a probe of the peripheral character of the reaction.

The superposition of different removed-nucleon + core-fragment configurations resulting after breakup creates a realistic picture of the original exotic projectile wave function. Therefore, the projectile wave function can be factorised as:

$$|Projectile\rangle = \sum_i A_i \big(|core\rangle \otimes |nucleon\rangle\big)_i , \tag{5.1}$$

where $|core\rangle$ and $|nucleon\rangle$ represent the core-fragment and removed nucleon wave function and A are the weighted probability[1] associated with each configuration. The detection of the gamma de-excitation of the fragment is used to discriminate different core configurations in the original projectile. Figure 5.1 left shows the reaction mechanism for the particular case of one-neutron knockout of a ^{23}O projectile by a light ^{12}C target.[2]

Different names have been used in the literature to refer to these kind of reactions (i.e.: nucleon removal, nucleon breakup and nucleon knockout). This last name was adopted by the NSCL scientists in their publications and is probably the most widely used (see review articles and references therein [1–3]). This term (knockout) was already used more than three decades ago to refer to Quasi-Free Scattering (QFS) reactions induced either by high energy protons and electrons, $(p, 2p)$ and $(e, e'p)$ [4, 5], and known to be very powerful spectroscopic tools. Figure 5.1 right shows the schematic representation of the quasi-free process induced by high energy exotic projectiles.[3]

QFS can be understood as a process in which a high energy particle knocks a nucleon out of a nucleus without any further significant interaction between the nucleon and the incident and the outgoing particles. After the reaction, and in the particular case of proton-knockout, the two protons (the target in our inverse kinematic example and the removed proton) emerge in the forward direction with a very strong

[1] Related to the spectroscopic factors.

[2] Reaction performed in inverse kinematics.

[3] Again illustrated by a reaction in inverse kinematics.

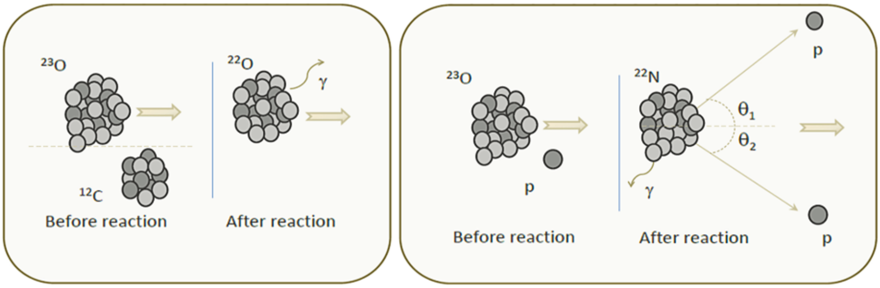

Fig. 5.1 *Left*: Schematic representation of a one-neutron knockout of an unstable ^{23}O projectile by a stable carbon target. A loosely bound neutron (not recorded) is removed during the reaction, leaving a core of ^{22}O. *Right*: Schematic representation of a quasi-free reaction induced by an unstable ^{23}O projectile on a proton target $(p, 2p)$. Two strongly correlated protons and the *A-1* fragment (^{22}N in this case) are emitted (and detected)

angular correlation.[4] The detection (momentum and direction) of both nucleons is necessary to provide kinematically complete measurements.[5]

Indeed proton-knockout using high-energy electrons $(e, e'p)$ was studied extensively in the 1980s, and was considered the only experimental method able to provide absolute spectroscopic factors in well-bound nuclei [6, 7]. QFS experiments are thus considered a quantitative tool for studying single-particle occupancies and correlation effects in the nuclei. They have been mostly exploited for reactions on stable nuclear targets and only very few QFS experiments to date involve rare species.

In this lecture, we will refer as knockout to the nucleon-removal from a projectile after reaction with a light target. The detection of the remaining fragment (with mass *A-1*) will be required but the knockouted nucleon will not be recorded. QFS will refer to reactions of a projectile with a proton (or electron). In this case, the detection of both nucleons (the removed one and the target) and eventually the *A-1* fragment is demanded and ensures fully exclusive measurements. It is our aim to provide an overview of the achievements and limitations related to the application of knockout and QFS reactions as spectroscopic tools for the particular case of exotic nuclei.

We would like to stress the complementary role of the different approaches so far discussed. Transfer reactions yield high cross sections (∼1 mb) at relatively low energies (in the range from few to 10–15 MeV/nucleon). The optimum range for knockout and QFS reactions are projectile energies ≈100 MeV/nucleon and higher. The cross section of the nucleon knockout process can vary from well above 100 mb, for loosely bound nuclei, to ∼1 mb for tightly bound nuclei. The cross section for the quasi-free channel, imposes a strong kinematical condition and it, is thus smaller and also depends on the separation energy of the removed nucleon, the removal of valence nucleons translates in larger cross sections.

---

[4]The two protons are emitted back-to-back ($\Delta\phi \approx 180°$) and with an average polar opening angle $\theta \approx 90°$.

[5]In some cases the fragment is also detected providing redundant information.

In the case of knockout reactions, the strong absorption concentrates the reaction probability at the surface, allowing mainly to probe the outer part of the projectile wave-function. The peripheral nature of the reaction is also true for both transfer and Coulomb breakup reactions. On the other hand, the use of QFS reactions induced by exotic projectiles on a proton target, allows one to determine the spectral functions of protons and neutrons (in the projectile) over a wide range, from the weakly bound valence nucleons to the deeply bound core states. These studies enable a more complete investigation of the projectile wave-function, giving access to different regions of a nucleus and probing different types of correlations that could exist within the nucleons.

The experimental possibility of working with high projectile energies can also be of particular interest. In a good approximation, at beam energies above 50–70 MeV/nucleon, the internal degrees of freedom of a nucleus can be considered "frozen" during the collision [8–10]. Only the nucleons directly participating in the interaction need to be taken into account in the theoretical description, the others are considered as simple spectators, thus simplifying the reaction mechanism description. The use of a semi-classical approximation of the reaction with regard to the impact parameter of the relative motion of projectile and target is permitted.

The production of high-energy secondary beams is achieved via in-flight projectile fragmentation (or fission) [11], using inverse kinematics, which means that the projectile is heavier than the target, having interesting kinematic consequences. The fragments produced are focused in the forward direction, which contributes to increase the overall transmission of these secondary beams to the secondary reaction target. These production mechanisms originate cocktail beams, formed by different isotopes. The selection of the nuclei of interest is done by help of powerful magnetic spectrometers [11] that identify "in-flight" the nuclear species, allowing the selection of a single isotope within the spectrometer's acceptance.

5.1.1 First Experiments

The shell model of the atomic nucleus was inspired by the atomic shell model. The main assumption of the nuclear shell model consists of a description of the nuclear interaction by a central potential with the ingenious idea of a spin-orbit coupling. To first order, each nucleon in a nucleus is assumed to move independently in a mean field resulting from interactions with the rest of nucleons. At the middle of last century the basis of this model was perfectly established [12, 13]. The major evidence of the adequacy of this orbital shell configuration came from the observation of magic numbers predicted by the model in stable nuclei, the only ones available for experimentation. Many experiments contributed to this important task, including those focused on the determination of energy spectra of the low-lying states, spins, magnetic moments, the observation of polarization effects of nucleons in nuclear collisions and the internal momentum determination of nucleons in proton and electron induced QFS reactions. Since then, the nuclear shell model is considered a cornerstone to describe the structural properties of nuclei.

Experiments of $(p, 2p)$ were first undertaken in 1952 in Berkley [14, 15] with the irradiation of protons on stable nuclei and the observation of coincident proton pairs, strongly correlated, emerging from the target. The interpretation of these experiments relied on the assumption that both the incident and the knocked-out proton were free. The angular correlation of the proton pair was interpreted as a consequence of the momentum distribution of the protons in the nucleus. Additionally, the separation energy distribution, evaluated for a given projectile particle, showed different structures (peaks) that were related to the binding energies of the various nuclear shells from which the protons were ejected. A number of experiments were then performed at Chicago, Harvard, Hawell, Orsay and Uppssala [16, 17], dedicated to the study of nuclei up to ^{40}Ca. The exploration of heavier nuclei, with smaller energy differences between shells and lower cross sections, was not addressed at this early stage. The poor energy resolution achievable in these experiments was the limiting factor.

Equivalent experiments employing high energy electrons appeared as an alternative, the nuclear transparency of the electrons was considered as an advantage. The distortion of the associated momentum distributions was expected to be much smaller and offered the possibility of studying inner shells. The drawback was that, these experiments required the development of powerful electron accelerators, providing intense beams to compensate for the small electromagnetic cross-sections. Very successful experiments of $(e, e'p)$ reactions were carried out in different facilities, for nuclei ranging from ^{2}H to ^{209}Bi. Profiting from the higher experimental resolution [4, 5, 18–21], transitions to many states in the resulting nucleus could be separated and the corresponding momentum distributions accurately measured.

The 80's became again a very exciting period with the advent of the first radioactive nuclei beams. The first experiments with radioactive secondary beams were performed more than fifty years ago ([22] and references therein). They concentrated on radioactivity experiments (i.e.: decay radiation, masses and determination of ground-state properties). Subsequent technological progress made it possible to apply techniques developed for stable beams to the case of secondary beams.

The advent of fast radioactive beams produced by projectile fragmentation and the development of the in-flight identification technique for the emerging fragments was an important milestone in the systematic study of unstable nuclei. The experimental access to nuclei away from the valley of stability enabled the discovery of many interesting phenomena such as dramatic changes in the neutron density at the surface of certain nuclei producing very low density tails (i.e.: nucleon halo or skin). The observed inversions and re-arrangements in the nuclear orbitals pushed an evolution of our traditional knowledge, demanding a revision of certain aspects of the traditional shell model, and were the driving force for an intense experimental and theoretical work to better understand the single-particle properties and the role of nucleon-nucleon (NN) correlations in these newly available exotic nuclei.

It is important to mention the pioneering work of Tanihata and collaborators in the systematic investigations of matter radii of exotic nuclei [23, 24]. A few years later, nucleon-knockout [25] was used for the first time to obtain spectroscopic information on unstable nuclei. Since then, this method has been used extensively. The first knockout experiments focused on the study of neutron-halo states and were later extended to other exotic species. The first cases investigated concentrated on lighter nuclei, mainly due to the technical limitations associated with the production of secondary beams. It is important to keep in mind that even today the neutron dripline[6] has only been reached for nuclei with low Z (up to $Z = 12$). Consequently, this is where most of the knockout experiments have been performed so far.

NSCL[7]/MSU in USA, was the first laboratory to implement the nuclear-knockout technique [26]. For many years, knockout experiments at NSCL have focused on the study of n-rich nuclei at intermediate energies (50–150 MeV/nucleon) [1, 3] (and references therein). They also pioneered the application of the knockout technique to the study of heavier nuclei [27] and have more recently extended their experimental studies to the removal of two nucleons [3, 28–33]. The knockout technique was also applied on several occasions [34–36] in GANIL[8] France, working on a slightly lower energetic domain (50–80 MeV/nucleon). Scientists at RIKEN[9] in Japan, concentrated on the study of Coulomb induced breakup [37, 38]. More recently, to coincide with the commissioning of RIBF[10] and BigRIPS[11] [39, 40] they undertook the investigation of very exotic isotopes using one and two neutron knockout [41]. The German laboratory GSI,[12] working in a higher energy regime (500–1000 MeV/nucleon), has carried out investigations on both Coulomb [42–44] and nuclear [45–55] induced knockout. All this work has contributed to modify the established picture of nuclei, proving that the nuclear orbital organization far from the beta stability is different. The importance of different effects (i.e.: the tensor force, pairing interaction, three nucleon forces, coupling to the continuum, etc.), might play a prominent role in these rare species, and offer new insights on the nuclear landscape.

QFS, can be also regarded as NN scattering channels in nuclear fields and thus could give a direct access to study the modification of nucleon properties in the nuclear medium, an interesting feature of nuclear physics not much explored so far. Experiments of $(p, 2p)$ reactions on different (^{6}Li, ^{12}C, ^{16}O and ^{40}Ca) targets [56] performed at RCNP[13] in Osaka (Japan) profited from high resolution detection of the two outgoing protons. They allowed to study knockout from deeply bound nucleon states. They also allowed, in the case of ^{12}C, a first measurements of the decay particles coming from deeply bound states, offering a qualitative comparison with the shell model and microscopic cluster calculations [57]. It is also worth to mention the electron-induced QFS experiments performed at Jefferson Lab (USA) in the last

[6]Limit of existence as a bound nuclear state.

[7]National superconducting cyclotron laboratory.

[8]Grand accélérateur national d'ions lourds.

[9]Nishina center for accelerator-based science.

[10]Radioactive ion beam factory.

[11]Separator and zero degree spectrometer.

[12]Helmholtzzentrum für Schwerionenforschung.

[13]Research center for nuclear physics.

decade. The analysis of the reaction of $^{12}C(e, e'p)$ reveals a large fraction of events that could be identified as proton-neutron pairs in ^{12}C. These events were interpreted as the result of the short-range component of the NN potential. The observation of a small amount of proton-proton and neutron-neutron pairs was also interpreted as a fingerprint of the tensor force [58].

Traditionally all these correlation effects and medium modifications have not been considered in the interpretation of direct reactions, but detailed studies have shown the eventual impact they could have. In the particular case of knockout reactions, this effect will not affect the shape of the momentum distribution[14] of the emerging fragment but would have an impact on the correct estimation of the cross-sections, particularly at low energies [59]. It is neither excluded, that the so-called "correlations" are simply the result of a insufficient description of the reaction mechanism.

The lecture is structured as follows. After this introduction, the main section is devoted to the analysis and interpretation of knockout reactions induced by radioactive beams, particularly in connection with their use as spectroscopic tools. We will finish with the presentation of the quasi-free channel induced by relativistic exotic nuclei on proton targets, which appears as an attractive extension of this kind of studies to probe the deeply bound states of rare species and offers the possibility of performing fully exclusive measurements.

5.2 Knockout Reactions

5.2.1 Extraction of Information in Knockout Reactions

In a knockout reaction a fast projectile with mass number *A* impinges on a target at rest (preferably light). The interaction projectile-target results in the removal of a single nucleon. It proceeds in a single step and is a very peripheral reaction, guaranteeing the survival of the *A-1* fragment. The study of knockout reactions in the laboratory occurs at relatively high energies (typically above 100 MeV/nucleon, even though many experiments have been done at lower energies ≈50–80 MeV/nucleon), where the use of semi-classical descriptions of the reaction mechanism is permitted. When describing the reaction mechanism of the knockout process, different contributions have to be considered.

- Stripping refers to cases where the removed nucleon reacts with the target, the nucleon is scattered to large angles and the target is excited.
- Diffraction or elastic breakup refers to reactions where the target remains in its ground state and the removed nucleon is emitted in forward direction.

[14] The momentum distribution themselves have a small dependence on the binding energy of the removed nucleon, but depend on the nucleon's orbital angular momentum, which enables identification of shell occupancy.

- A third contribution, called Coulomb dissociation, corresponds to electromagnetic elastic breakup and plays a minor role in the case of light targets, as it is the case of the reactions that will be described in this paper, and thus will not be discussed in detail.

Within this scenario the cross-section can be expressed as:

$$\sigma = \sigma_{strip} + \sigma_{diff} \tag{5.2}$$

Depending on the beam energy, the relative importance of each process is different. At high beam energies the one-neutron removal cross-section is dominated by stripping whereas at lower energies, 50–60 MeV/nucleon, both contributions are similar [60]. As a general statement, the use of direct reactions as a spectroscopic tool demands a very detailed and realistic description of both the nuclear structure and the reaction mechanism.

In the case of nucleon knockout, the reaction mechanism has been often given by the (semi-classical) eikonal approximation, providing a geometrical description of the reaction in terms of the impact parameter of the relative motion of projectile and target. The strong point of the eikonal description is the relative simplicity associated with both the calculations involved and the required physical inputs. For the single step assumption to be valid, sufficiently high energies must be employed to allow for the use of the adiabatic approach, in which the internal motion of the nucleons inside the nucleus is neglected during the collision [8, 10]. The nucleons not directly involved in the reaction are considered simply as "spectators". As it will be shown in the following sections, many knockout experiments can also determine spin and parity (I^{π}) of the remaining fragment from the measurement of the γ de-excitation of the fragment, enabling exclusive measurements to given states (n, l, j).

There are many references describing in detail the eikonal methods [1, 8, 9, 61–63]. We will illustrate in this section the case of a system that follows a nucleon-knockout reaction, described by the subsystems after breaking: the core-target and the nucleon-target [42, 63]. The cross-sections can be calculated as follows:

$$\sigma_{diff} = \int d\mathbf{b}\big[\big\langle\big|(1 - S_c S_n)\big|^2\big\rangle - \big|\big\langle(1 - S_c S_n)\big\rangle\big|^2\big] \tag{5.3}$$

$$\sigma_{strip} = \int d\mathbf{b}\big\langle\big(1 - |S_n|^2\big)|S_c|^2\big\rangle \tag{5.4}$$

The cross-sections are expressed as a function of the profile functions S [64, 65], linked in the eikonal model to the scattering matrix and evaluated from the eikonal phase-shifts. The profile functions for the core-target (S_c) and nucleon-target (S_n) depend on the impact parameter and are calculated using density distributions that reproduce measured cross-sections (see [42] for the particular case of ^{11}Be neutron-knockout). The theoretical cross-sections for each of the above mentioned processes, can thus be calculated individually for the occupancy of each subshell orbital for a given state (n, l, j), relating to the single-particle cross section for each subshell at that energy.

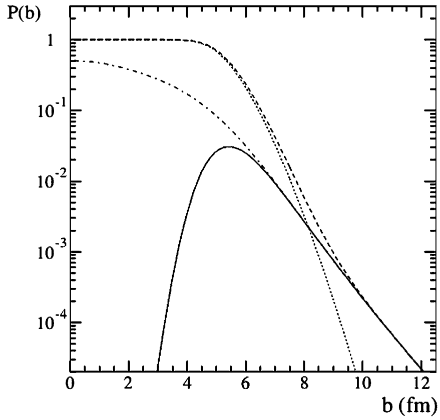

Fig. 5.2 Probability evaluation for one-neutron knockout in ^{17}O ($d_{5/2}$ neutron with $S_n = 4.1$ MeV). The *dashed curve* represents the total reaction probability. The *dash-dotted line* is the neutron reaction probability, i.e.: $\langle 1 - S_n^2 \rangle$, whereas the *dotted line* corresponds to core survival probability, i.e.: S_c^2. The *solid line* is the neutron reaction probability times the core-survival probability [68]

Other authors have worked with descriptions providing a pure quantum treatment of the reaction (the eikonal makes use of a classical description for the projectile movement). These approaches can only account for the elastic (or diffractive) term, ignoring the stripping that can be important in these reactions. Some attempts of using these approaches can be found in Refs. [66, 67].

Using the eikonal approach, we can also probe the peripheral character of this kind of reactions. If one assumes identical impact parameter for both projectile and core,[15] the core-target profile function can be taken outside the expectation value and the probability evaluation can reduce to

$$P(\mathbf{b}) = S_c^2(\mathbf{b})\big\langle 1 - S_n^2(\mathbf{b}_n)\big\rangle = S_c^2(\mathbf{b}) \int d^3r \left|\phi_{nlj}(\mathbf{r})\right|^2 \left[1 - S_n^2(\mathbf{b}_n)\right], \tag{5.5}$$

with ϕ_{nlj}, the single-particle wave function of specific states, expressed as a function of the relative core-nucleon distance. The terms involved in this expression represent the reaction probability of the nucleon with the target ($\langle 1 - S_n^2 \rangle$), and the survival of the core S_c. This calculation allows for instance to evaluate the one-nucleon knockout with a given orbital angular momentum, and is very helpful to understand the surface dominance of this kind of reaction. Figure 5.2 shows an example of the probability evaluation for the case of ^{17}O considering the knockout of a $d_{5/2}$ neutron [68]. One can observe a concentration of the neutron knockout probability at the nuclear surface.

To compare the evaluated single-particle cross-sections with the experimental ones, the former need to be normalised by the spectroscopic factor (C^2S), associated with each occupied subshell for this particular state. The result provides the theoretical cross-section (see (5.6)) for the removal of a nucleon from each of the considered subshells for this state which, when they are summed, yield the theoret-

[15] No recoil limit.

ical cross-section for neutron removal from this state.

$$\sigma_{theo} = \sum_j C^2 S(I_\pi, nlj)\sigma_{sp}(nlj) \quad (5.6)$$

The sum, for all bound states, yields the complete theoretical cross section for the reaction channel under the particular conditions considered (target, beam energy, etc.). Section 5.2.3.1 includes examples of these kind of calculations applied to the ^{11}Be and ^{8}B case.

A spectroscopic factor is formally defined as the overlap of two many-body shell-model wave functions, corresponding to the initial nucleus (*A*) and the emerging core (*A-1*) in the case of nucleon-knockout. Computation of the spectroscopic factors requires a shell model calculations, the reader can find further information on the shell model in almost any nuclear physics text book. This subject has also been treated in the Euroschool notes by H. Grawe [69] and T. Otsuka [70]. Different codes are available on-line [71–73] and can be used for simple computations.

When using C^2S to weight the single-particle cross-sections, C^2S are interpreted as the intensity related to the core state (Φ_{A-1}), and thus as the pre-existing weight of a given component ($|core\rangle \otimes |nucleon\rangle$) in the incident projectile ground state wave function (Φ_A).

The comparison of the theoretical cross-section, including C^2S, and the measurement would also allow to determine the factor S (also named R_S), interpreted as an experimental spectroscopic factor.

$$\sigma_{exp} = S\sigma_{theo} \quad (5.7)$$

In a typical knockout experiment, the measurement of the remaining fragment momentum distribution, allows for the determination of the angular orbital momentum l of the removed nucleon. Taking the "adiabatic approximation" and keeping in mind the momentum conservation, the momentum of the recoil fragment after one-nucleon removal provides a measurement of the momentum of the removed nucleon. In the centre of mass system both quantities have equal modulus and opposite directions.

The shape of the momentum distribution is related to the Fourier transform of the radial wave function. It is also well known that the spatial extension of this radial wave function could be very different depending on the orbital angular momentum. In general, a lower orbital angular momentum yields a very extended spatial extension and thus a narrow momentum distribution. Figure 5.3 shows the example of radial wave functions associated with different l values and the corresponding momentum distributions applied to the ^{17}O example.

We can conclude that the shape of the residual fragment momentum distribution is dependent upon the orbital angular momentum components of the removed nucleon. The comparison of the experimental and evaluated momentum distribution thus allows the discrimination of the l of the knockout nucleon. This signature is analogue to the one extracted from the angular distributions in transfer reactions.

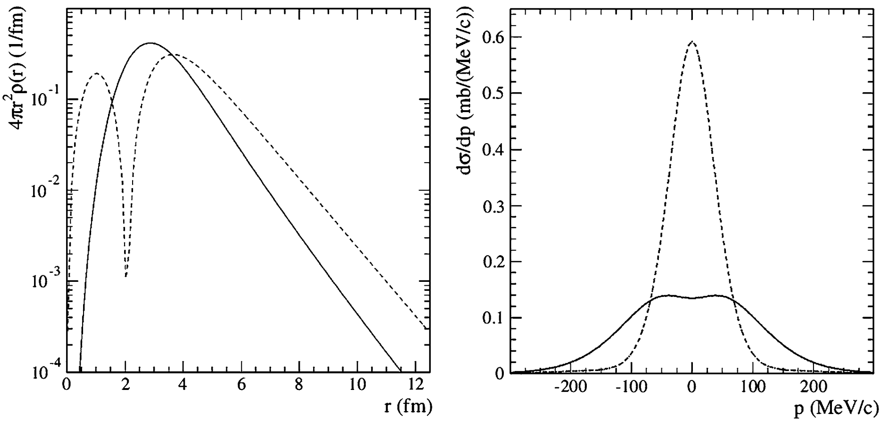

Fig. 5.3 Calculations performed for ^{17}O ($|^{16}\text{O}\rangle \otimes |n\rangle$). *Left*: Radial wave function for neutrons with different orbital angular momenta ($s_{1/2}$ represented by the *dashed line* and $d_{5/2}$ with *solid line*, in both cases $S_n = 4.1$ MeV). *Right*: Longitudinal momentum distribution of a remaining fragment after one-neutron knockout (^{16}O) associated with the two radial wave functions shown in the *left panel* [68]

One must remember that the independent-particle shell model relies on the assumption that each nucleon moves independently of the rest of nucleons in a nucleus. Indeed, they are not free nucleons, but subject to the action of an average potential (mean-field) induced by the neighbouring nucleons. In the nuclear shell model picture deeply-bound states are seen as fully occupied by nucleons. At the Fermi energy level (and above), configuration mixing can lead to reduced occupancies that gradually decrease to zero. The evaluation of S (R_S), and its deviation from unity, can be understood as a possible quantification of different correlation effects that are beyond the effective interactions used in the shell-model to "build" the mean-field. These kind of effects have been known for many years, observed from data of electron induced $(e, e'p)$ quasi-free scattering using stable beams with A ranging from 7 to 208, which probed the structure using knockout in both valence and deeply bound orbits (see [5] and Fig. 5.4). They show an average S value on 0.6–0.7. These data on stable nuclei can be completed with other coming from nucleon knockout of exotic projectiles (presented in detail in Sect. 5.2.3.5).

It is also worth to mention the efforts to evaluate spectroscopic factors with sophisticated calculations based on ab-initio methods which incorporate two-and three body interactions [74–78]. These calculations are only possible for the case of light nuclei.

5.2.2 *Experimental Needs and Relevant Observables*

The success of the nucleon knockout technique relies on two main premises:

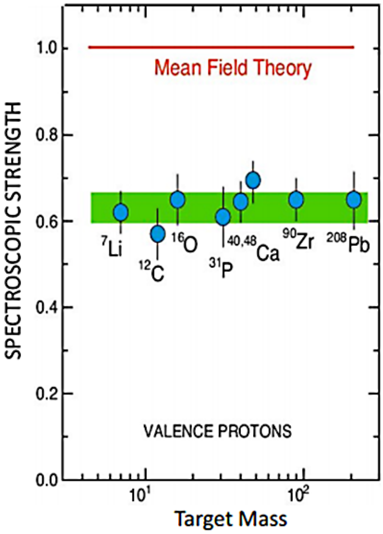

Fig. 5.4 The $(e, e'p)$ data for quasi-free scattering of valence and deeply bound orbits in nuclei gives experimental spectroscopic factors that are 60–70 % of the mean field predictions [5]. Figure extracted from [5]

(a) the use of high-energy secondary beams in conjunction with thick targets provides an efficient enhancement of the reaction yields. Reactions at high energy present an additional advantage of emitting the reaction products in a forward focused cone, offering a rather high efficiency with moderate size detectors.
(b) a detection system able to select the reaction channel and ensure a kinematically complete measurement (i.e.: identification and tracking of projectiles and core-fragments, high precision measurement of the core-fragment momentum and discrimination of the different possible core-fragment excited states).

Currently, high-energy secondary beams are produced by projectile fragmentation of stable beams that are generated by heavy ion accelerators such as synchrotrons and cyclotrons. Projectile fragmentation results in a cocktail beam composed of the various fragments produced. The intensity of the secondary beams must be sufficient to guarantee the success of the experiment: a minimum intensity of a few particles per second is necessary to perform inclusive exploratory investigations. This intensity will depend on different factors. The most important are:

– the type of accelerator used: cyclotrons generally provide higher intensities than synchrotrons. At the time of writing, the largest secondary beam intensities are achieved in RIBF [40, 41] (Japan). An important intensity upgrade is expected with the arrival of the new FAIR[16] [79] (Germany) and FRIB[17] [80] (USA) facilities in the future.
– the choice of projectile: the closer the primary projectile and the secondary beams are in A and Z, the higher the production cross section.

[16]Facility for antiproton and ion research.

[17]Facility for rare isotope beams.

– the target thickness: working at high energies makes it possible to use relatively thick targets, which have a larger number of atoms and thus a greater secondary particle yield.

Many knockout experiments rely on the use of very powerful magnetic spectrometers. These devices are composed of a set of electric and magnetic elements that guarantee optimum transport of secondary projectiles and emerging fragments. Electromagnetic spectrometers also act as filters allowing unambiguous identification of secondary fragments from amongst all the species produced following fragmentation of the projectile. They are equipped with various detectors to ensure identification and tracking of ions traversing the system on an event-by-event basis. Last but not least, spectrometers provide a very accurate determination of the momentum of the nuclei from the accurate measurement of the position distribution. Interested readers will find further details on these topics in Refs. [11, 81, 82].

Using knockout, the observables that provide experimental access to the exotic projectile wave function are the momentum distribution of the surviving core-fragments following nucleon knockout and the cross section associated with this reaction channel. The longitudinal momentum distribution of the core-fragment provides information about the wave function of the removed nucleon, whereas spectroscopic factors (C^2S) determined from the removal cross sections to each (n, l, j) state, represent the occupancies of the subshell orbitals in the model space considered for each state. Gamma de-excitation of the core-fragment can also be measured with gamma detection arrays. The coincident detection of core-fragment momentum distribution and removal cross-section with gamma-rays provides information on each individual contribution to the exotic projectile wave function. As a general rule, the removed nucleon is not detected. Only some experiments have concentrated on the detection of the removed nucleon allowing the experimental determination of the cross-section for each reaction mechanism (diffraction and stripping) and validating the reaction models so far used. In the rest of cases, direct discrimination of the removal mechanism is not possible and is taken into account by the reaction model.

Figure 5.5 shows a schematic view of the generic experimental setup at the FRagment Separator (FRS) at GSI [83]. The determination of all the observables introduced in this section is referred to in this example. Other devices extensively used to perform measurements of this kind are the A1900/S800 spectrograph at NSCL/MSU [84], the BigRIPS at RIBF/RIKEN [39, 40] and the SPEG energy loss spectrometer at GANIL [85].

The first section of the spectrometer is tuned to separate from the primary beam and transport the nucleus of interest to where the beam is focused at the intermediate image plane. Here a target is placed, where the knockout reaction is induced. Other fragmentation products within the spectrometer acceptance will be transported as well (as shown in the left panel of Fig. 5.6). The spectrometer section behind the knockout target is then tuned to the magnetic rigidity of the $^{A-1}$X fragments produced in the one-nucleon knockout reaction (right panel of Fig. 5.6).

It is essential to ensure an unambiguous selection of the reaction channel. This is achieved via the double identification of the exotic projectile in front of the knockout target and the remaining core-fragment following the reaction. Figure 5.6 illustrates

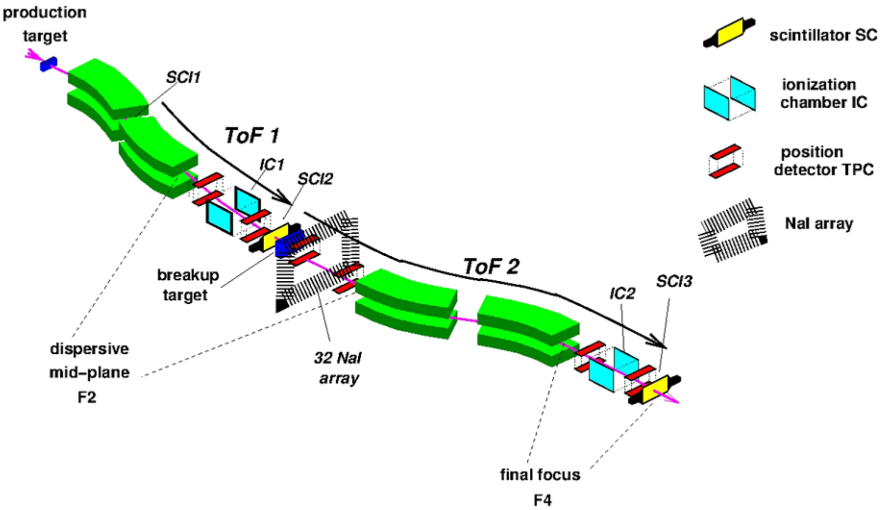

Fig. 5.5 A schematic view of the FRagment Separator (FRS) with its detection set-up. Complete identification with ToF (SC) and energy-deposition (IC) measurements is possible in both sections of the spectrometer. Several position sensitive detectors (TPC) provide projectile and fragment tracking as well as the measurement of fragment momentum distributions. A γ detector (NaI) provides the coincident measurement of fragments with prompt γ-ray deexcitation

a particular case corresponding to the ^{40}Ar fragmentation at 1 GeV/nucleon performed at the FRS. The first section of the spectrometer was tuned to select ^{20}O fragments (right panel), whereas the second section was tuned to select ^{19}O fragments emerging from one-neutron knockout reactions on a carbon target. In this particular measurement, identification was achieved by determining the A/Z ratio from Time of Flight (ToF) measurements with plastic scintillators, and energy losses ($\propto Z^2$) recorded by ionisation chambers.

As it was mentioned earlier, in the "adiabatic" approximation, the momentum of the core-fragment following one-nucleon removal provides information on the wave function of the removed nucleon. Narrow momentum distributions have been associated with a large spatial extension of the removed nucleon (associated with low angular momentum).[18] This was clearly observed in experiments with halo nuclei that will be presented in detail later in this lecture (Sect. 5.2.3.1). The core-fragment momentum is determined by measuring the velocity shift induced by the knockout target. To determine this velocity shift, position sensitive detectors measure the position distribution of the one-nucleon removal residue at the final focal plane.

It is important to keep in mind that the experimental determination of core-fragment momentum distributions requires high-resolution measurements. The most stringent cases would correspond to the narrow momentum distributions of halo nu-

[18] The FWHM of the momentum distribution due to knockout is around 50 MeV/c for an s ($l = 0$) neutron, and around 300 MeV/c for a d ($l = 2$) neutron.

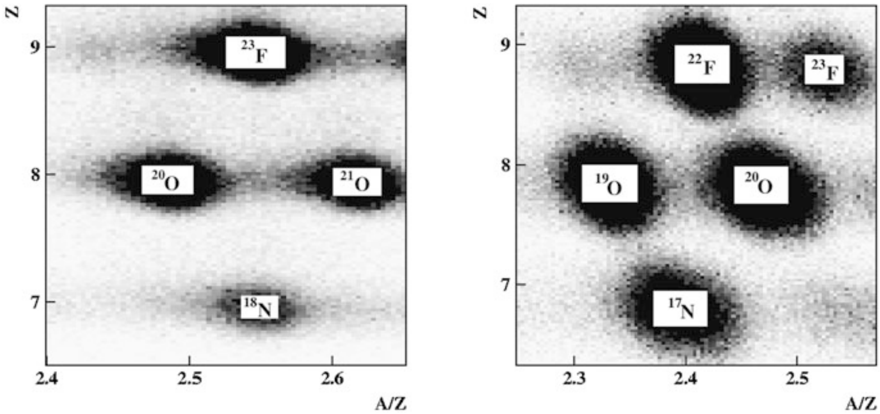

Fig. 5.6 Identification of different secondary beams (*left*) and the corresponding one-neutron removal core-fragments (*right*) emerging after one-neutron knockout on a carbon target. This cocktail beam was obtained by fragmentation of ^{40}Ar at 1 GeV/nucleon impinging on a Be target [48]

clei (see Sect. 5.2.3.1), where a single-particle hole yields a FWHM of the order of 50–80 MeV/c in the core-fragment momentum distribution.

Position distribution measurements are possible in the transversal beam directions. These quantities make it possible to determine the longitudinal (parallel) and transverse (perpendicular) contributions with respect to the beam direction of the core-fragment momentum distribution. Both projections should contain the same information but the longitudinal distribution is preferred because it is less affected by Coulomb diffraction and diffractive scattering mechanisms.

From now on, core-fragments momentum distributions will always refer to the longitudinal component. The experimental determination of the core-fragment momentum distribution is measured in the laboratory reference system and then transformed to the projectile frame using the corresponding Lorentz transformation.

The final core-fragment momentum resolution depends not only on the tracking and magnetic resolving power but also on the quality of the projectile beam (spot size and angular alignment) and the amount of matter at the mid-plane (angular energy straggling). Most of these contributions can be experimentally evaluated by measuring the momentum distribution of the projectile (without knockout target) [45, 86], which can be used for deconvolution (FWHM reported in the literature are always corrected by this value). Figure 5.7 shows these effects for the case of ^{19}C at 910 MeV/nucleon. Another possibility to get free of the effects non due to the knockout reaction on the momentum distribution would consist on the determination of the projectile incoming angle that could be subtracted on an event-by-event basis, to obtain a corrected outgoing angle for the emerging fragment.

The left panel in Fig. 5.8 shows core-fragment momentum distributions of different carbon projectiles, at almost 1 GeV/nucleon, following one-neutron knockout ranging from the bound nucleus ^{12}C with a FWHM of 220 ± 12 MeV/c to the loosely bound nucleus ^{19}C with a FWHM of 71 ± 3 MeV/c. These experimental results reveal the different initial state of the removed neutron, and indicate the dominance of

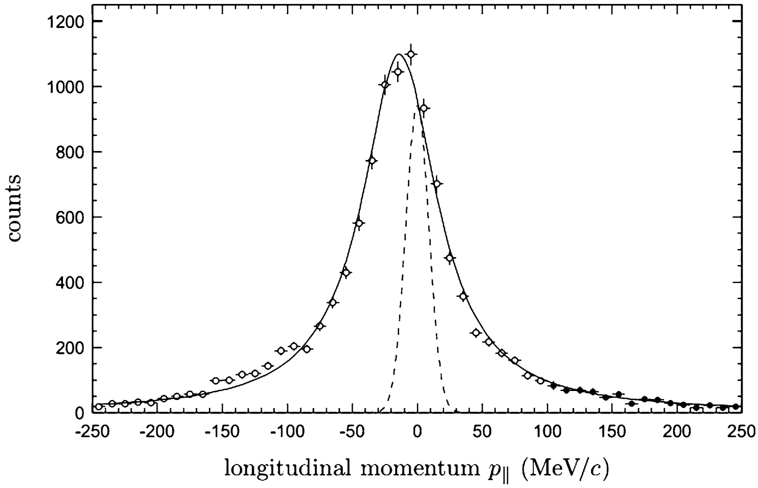

Fig. 5.7 Measured longitudinal momentum distribution of ^{18}C fragments from one-neutron knockout of ^{19}C at 910 MeV/nucleon on a carbon target (*points*). The *dashed profile* represents the measured system resolution with a width of 19.9 MeV/c [86]

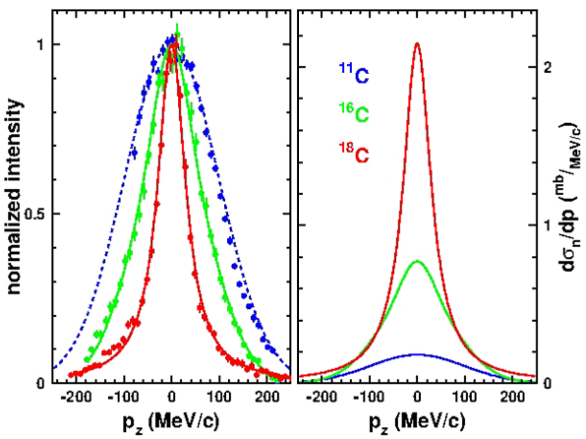

Fig. 5.8 Longitudinal momentum distributions of different carbon fragments, at ≈910 MeV/nucleon, emerging from one-neutron knockout reactions, normalised to the unit (*left*) and to the measured removal cross-sections. Data taken from [45, 86]

s-wave occupancy in the ground state configuration for the one-neutron halo nuclei ^{19}C [45].

The one-nucleon removal cross section is deduced from the ratio between the number of incoming exotic projectiles and the number of knockout residues. This last quantity is determined at the final focal plane of the spectrometer and must be corrected for the corresponding fragment transmission in the spectrometer region between the knockout target and the detection point. This transmission is evaluated by means of simulation programs that account for the ion-optical transport of the nuclei through the spectrometer (i.e.: LISE [87], MOCADI [88]). Other corrections, such as secondary reactions in the knockout target, detector efficiency and

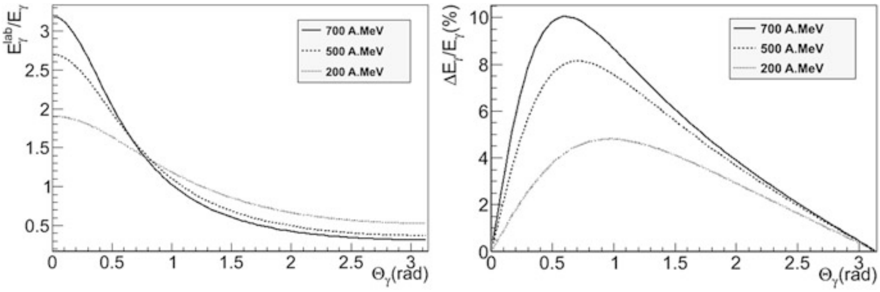

Fig. 5.9 Doppler shift and Doppler broadening for gamma-rays emitted by relativistic sources at different energies (curves generated for detectors with angular segments of about four degrees)

data acquisition dead time are also considered. The right panel of Fig. 5.8 shows the measured momentum distributions for the different C isotopes, normalized to the corresponding cross sections. These two observables, core-fragment momentum distribution and nucleon removal cross section, are determined independently.

For exclusive measurements of these observables for the bound excited states, the experimental setup must provide information on core-fragment de-excitation after knockout. The most common method for distinguishing the different core-fragment configurations contributing to the exotic nuclei wave function, requiring to differentiate between core-fragment in the ground state and in excited states, is via the coincident detection of the surviving core-fragment with a gamma ray emitted in the de-excitation process. Therefore, the gamma-ray detector must be located near the knockout target. Different gamma detector arrays are used. The first experiments were performed with scintillation-based detectors (namely NaI(Tl) and CsI(Tl)) with moderate intrinsic energy resolution. These have been gradually replaced by Ge detectors which have an excellent intrinsic energy resolution, but considerably smaller efficiency in detecting high energy gamma-rays.

The recorded gamma-ray spectra, emitted by relativistic sources would be subject to the Doppler effect (shift and broadening). The Doppler shift represents the gamma energy transformation between the laboratory and centre of mass reference systems. The left panel in Fig. 5.9 shows the evolution of the Doppler shift with the polar angle. For the forward angles ($\theta < 40$ degrees), this effect significantly increases the energy in the laboratory system, which results in lower gamma-detection efficiency (the detection efficiency of a gamma detector depends on the gamma energy, the higher the gamma energy the lower the efficiency). Doppler broadening reflects the effect of the angular aperture of the gamma detector in the final energy resolution of the system. The right panel of Fig. 5.9 shows the evolution of this effect with the polar angle (for a given detector angular aperture). The energy resolutions shown in this picture are calculated without considering the intrinsic energy resolution of the gamma detector used. We can also see (in Fig. 5.9) that the Doppler shift and broadening become more pronounced as the energy of the emitter increases. The Doppler shift can be corrected by determining the velocity of the emitter and the gamma-ray emission angle. However, the broadening effect is determined by the velocity

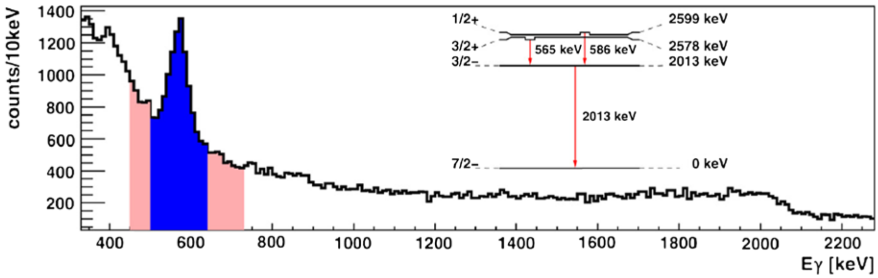

Fig. 5.10 Gamma rays recorded from the ^{47}Ca core-fragment de-excitation following the reaction ^{9}Be(^{48}Ca, ^{47}Ca + γ)X at around 500 MeV/nucleon. Data recorded with MINIBALL Ge array in the intermediate focal plane of the FRS [90]

of the emitter and the detector angular aperture, and cannot be corrected. The final energy resolution will be dominated by this kinematic broadening. Thus, detector segmentation becomes a key factor, the finer the segmentation the better the energy resolution. These "weak" points, i.e.: small efficiency for energetic gamma-rays and finite angular segmentation, limit the performance of gamma arrays, particularly at high-energies, and constitute difficult challenges in the determination of exclusive observables.

Figure 5.10 shows an example of a gamma energy spectra recorded with the MINIBALL [89] Ge array in the intermediate focal plane of the FRS. The experiment aimed to probe the single particle properties around ^{54}Ca [90] (^{47}Ca depicted here was used as the reference case), where a shell closure effect for $N = 34$ ($Z = 20$) was predicted [91]. In this case, the emitter energy was ≈500 MeV/nucleon ($\beta \approx 0.76$). We can observe in this figure that the energy resolution achieved for the peak ≈570 keV is around a few percent. This energy resolution is considered a good result for in-beam gamma ray spectroscopy for relativistic moving sources, but it is nowhere near the intrinsic energy resolution of these Ge detectors (well below 1 %). Another example of γ-detection with segmented Ge detectors is shown in Fig. 5.17 for a moving source at 80 MeV/nucleon.

The detection of gamma-rays at very high energies (500–700 MeV/nucleon) remains a critical issue that will improve in the near future with the construction of dedicated detectors. Special mention deserves CALIFA [92], a spectrometer/calorimeter under construction for the R^{3}B/FAIR [93] experiment. CALIFA, with more than 3000 detection units, based on highly performant CsI(Tl) crystals read-out by Large Area Avalanche Photo Diodes,[19] will reduce the impact of Doppler broadening on the final energy resolution, providing $\Delta E/E \approx 5$ % at 1 MeV ($\beta \approx 0.7$) and an overall photo-peak efficiency of 40 % for γ rays up to 15 MeV (in the projectile frame).

Experiments addressing the detection of the knockout nucleons have not been so numerous. They are however very interesting to discriminate between different

[19] Option adopted for the backward angles of CALIFA.

reaction mechanisms. Among these exclusive experiments, some have concentrated on the detection of the diffractive component [38, 42, 94–96].

Special mention is due to the work of Bazin and collaborators [67] who reported a detailed study of the relative importance of the stripping and diffraction mechanisms involved in the one proton removal reaction, using a coincident measurement of residue and knockout proton. In typical knockout experiments, the removed nucleon is not detected and the reaction theory is used to estimate the relative weight of elastic and inelastic removal mechanism. Later these contributions are summed up and compared with the experimental result. The validation of the reaction mechanisms requires exclusive measurements detecting both momenta, one associated with the heavy residue and the other to the removed nucleon. This was successfully achieved in the one-proton knockout of ^{9}C and ^{8}B on a Be target at an incident energy of ≈150 A MeV [67]. The reactions took place in the scattering chamber of the A1900/S800 [84] spectrograph. This apparatus was also used to collect and identify the one-proton fragments around zero degrees, whereas the light particles emerging at large angles were measured with the HiRA [97][20] detector array (a telescope consisting in two layers of Si and CsI). The relative contribution of both reaction mechanisms was deduced from the energy sum spectra of both heavy and light fragments in coincidence (see Fig. 5.11) and showed an excellent agreement with the values predicted by the eikonal model, giving confidence for the correctness of using knockout reactions as tool to determine single-particle spectroscopic strengths in exotic nuclei.

5.2.3 Results of Knockout Measurements

Knockout experiments employing inverse kinematics started in the early 90's. The first experiments were relatively simple and consisted of the single detection of the emerging *A-1* fragment. These kind of experiments were called "inclusive" and could not distinguish neither the post-reaction fragment excitation nor the contributions due to stripping or diffraction. Soon it became evident that detailed studies were required and the coincident gamma de-excitation of the fragment began to be present for almost any knockout experiment. The discrimination on the reaction mechanism relied on the description of the reaction theory and only few experiments concentrate on the detection of the knockout nucleon. Both cases, the coincident detection of the fragment gamma de-excitation and the detection of the knocked out nucleon constitute what we know as "exclusive" measurements.

In some cases, by profiting from cocktails beams it was possible to study many different species simultaneously. Figure 5.12, shows results [98] obtained at the FRS(GSI), of inclusive momentum distributions of residual nuclei after one-neutron knockout, superimposed upon a chart of the nuclides. In this picture, the vertical axis

[20]HIgh resolution array.

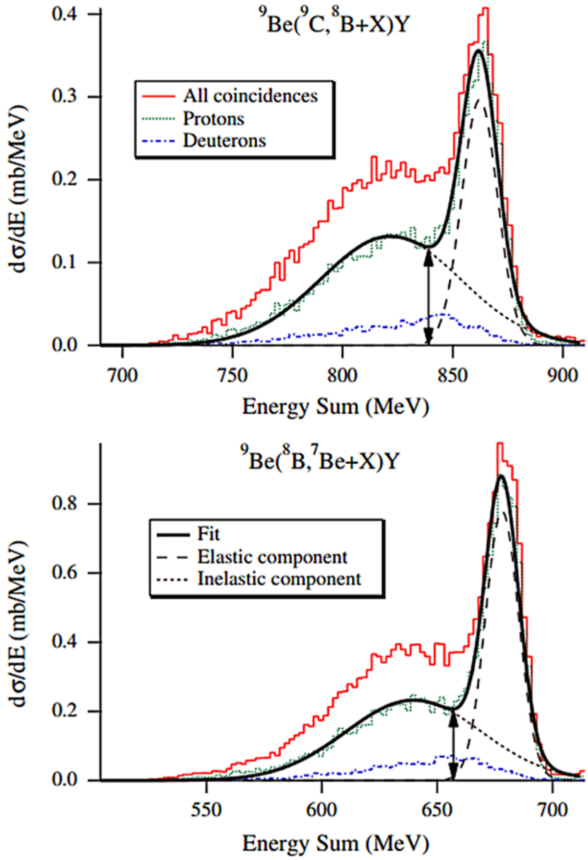

Fig. 5.11 Energy sum spectra of one-proton knockout for ^{9}C (*upper panel*) and ^{8}B (*bottom panel*). The inelastic and elastic components of the fit are used to evaluate the exclusive contributions [67]

corresponds to the Z number and the horizontal axis to the N number of the exotic projectile before fragmentation. Several neutron-rich isotopes could be investigated in a single experiment where a cocktail secondary beam was produced by nuclear fragmentation of ^{40}Ar at 700 MeV/nucleon. Though qualitative, the evolution of the momentum distribution in this figure reflects the structural changes encountered by nuclei approaching the dripline. For example one can observe the narrowness of the distribution for well known "halo states" such as ^{19}C, or the $N = 14$ sub-shell effect (^{22}N, ^{23}O, ^{24}F, ^{25}Ne, ...). This figure also reveals the potential of this technique to perform exploratory investigations, as indicated by Sauvan et al. [35, 36]. The information provided by the ensemble of data obtained, in different facilities and at different energetic domains over the last 25 years is quite coherent.

In the following sections we present a selection of different experimental works that provide the reader with a picture of the progress achieved so far. They are organised in different subsections which highlight different subjects of interest. The limitations and difficulties encountered will be also commented.

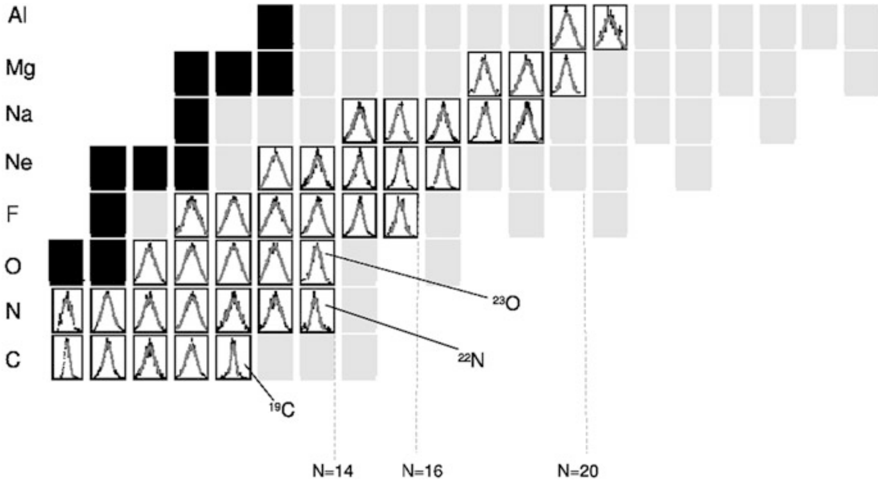

Fig. 5.12 Inclusive longitudinal momentum distributions of the *A-1* fragments after one-neutron removal from the various projectiles indicated on top of a chart of nuclides. *Black squares* correspond to stable isotopes. The measurements were performed at GSI using beam energies around 700 MeV/nucleon [98]

5.2.3.1 Study and Characterisation of Halo States

Near the neutron dripline the large neutron excess and the small neutron binding energy can lead to unexpected changes in the nuclear structure. Through the years, special attention has been given to the case of nuclear halo states. When approaching the driplines the separation energy of the last nucleon, or pair of nucleons, decreases gradually and the bound nuclear states come close to the continuum. In some cases, the combination of the short range of the nuclear force and the low separation energy of the valence nucleons results in considerable tunnelling into the classical forbidden region and a more or less pronounced halo may be formed. A halo nucleus can be visualized as an inert core surrounded by a low density halo of valence nucleon(s) [99–101]. The formation of halo states is especially characteristic for light nuclei in the dripline regions, although not all of these can form a halo.

Analysis and interpretation of knockout experiments dedicated to the study of "halos" has undoubtedly led to a better understanding of the knockout technique and its development and application as a powerful spectroscopic tool. In earlier experiments, the experimental signatures of these phenomena were the narrow momentum distribution of the emerging fragments after one-neutron knockout, reflecting the large spatial extension of the removed nucleon, and the large one-neutron removal cross sections that constitute a complementary source for structure information (see [99] for a detailed compilation). These first experiments relied uniquely on the detection of the core-fragments and are known as "inclusive" measurements. However, we should not forget that the nuclei under study are located far away from the beta-stability line and that the resulting core-fragments are exotic nuclei themselves. As a result, core-polarisation effects are quite common. Indeed, soon it became evident that a non-negligible fraction of the measured neutron-removal cross section was populating excited states in the residue. This meant that the observed longitudinal momentum distributions were in reality the superposition of broad components associated with core-fragment excited states onto the narrow distribution associated with the halo states (mainly in the core-fragment ground state).

The use of gamma-ray coincidence, mentioned earlier, made it possible to separate these different contributions which in turn made it possible to determine the partial cross-sections of the different core states. The observables extracted under these conditions are referred to as "exclusive". This exclusive experimental information, together with an adequate model describing both the structure of the nuclei involved and the reaction mechanism, allows for the experimental determination of spectroscopic factors. This coincidence technique is not exempt from experimental problems. Cases involving nuclei with complex decay schemes, and/or with many weak transitions would be associated with larger experimental errors that would make a detailed analysis difficult or impossible. However, as in the case of "halos", nuclei close to the driplines exhibit very few bound states making this determination easier.

In the following paragraphs, we will concentrate on the description of two well-known cases, ^{11}Be and ^{8}B, which correspond to one-neutron and one-proton halo states, respectively.

- One-neutron halo ^{11}Be

  Our first example is ^{11}Be with only three bound excited states and a one-neutron separation energy of ∼500 keV. The ground state of ^{11}Be, considered as a $1/2^+$ intruder from the sd shell, is a well known one-neutron halo state. First experimental evidences of it came from the measurement of the half-life of the 320 keV excited state of ^{11}Be, suggesting an extremely strong E1 transition [102], and the narrow momentum distribution of ^{10}Be core-fragments resulting after one-neutron knockout of ^{11}Be [103]. The initial picture of an inert ^{10}Be core and a neutron in a $1s$ shell, soon gave way to a more complex picture where the pertinence of this inert core was questioned.

  The most favourable scenario consisted of an admixture of a neutron in a $0d_{5/2}$ orbital coupled to the first excited state in ^{10}Be (2^+), but theoretical predictions ranged in their estimates from 7 % to 40 % [104, 105]. The experimental situation was ambiguous, with different results from ^{10}Be$(d, p)^{11}$Be experiments providing quite different spectroscopic factors [106–108], some of them incompatible with earlier Coulomb dissociation experiments [109, 110]. The knockout experiment performed by T. Aumann et al. [111] at NSCL (A1900/S800) shed light on this question. They produced a secondary beam of ^{11}Be at 60 MeV/nucleon via nuclear fragmentation of ^{16}O. The ^{11}Be beam impinged on a Be target producing the one-neutron knockout. A NaI(Tl) array located around the removal target recorded the gamma-rays in coincidence with the ^{10}Be fragments, which were analysed with the tracking detectors located at the end of A1900/S800 [84] (see experimental details in [111]). The resulting gamma-energy spectrum is displayed

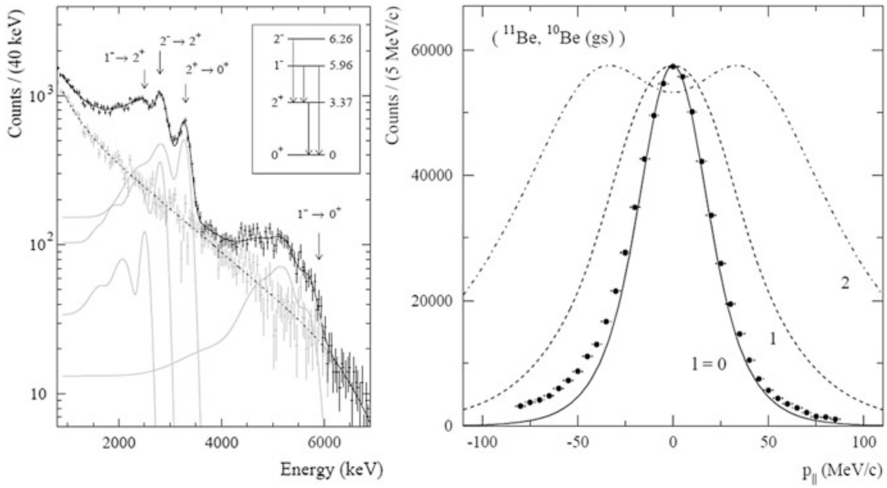

Fig. 5.13 *Left*: Doppler-corrected gamma energy spectrum measured with the NaI array in coincidence with ^{10}Be core-fragments emerging from the ^{9}Be(^{11}Be, ^{10}Be + γ)X one-neutron knockout. *Right*: Longitudinal momentum distribution of the ^{10}Be ground state fragments. The *curves* are calculations assuming a knockout reaction from s, p, and d states [111]. Pictures taken from [111]

Table 5.1 Partial cross sections (mb) to all final states I^π observed in ^{10}Be after one-neutron knockout from ^{12}Be. Different contributions of theoretical single-particle cross sections in the eikonal model are reported. The sum multiplied by the spectroscopic factor is compared with the experimental values [111]

I^π	l	C^2S	σ_{sp}^{knock}	σ_{sp}^{diff}	σ^{other}	σ^{theo}	σ^{expt}
0^+	0	0.74	125	98	10	172	203(31)
2^+	2	0.18	36	14	11	11	16(4)
1^-	1	0.69	25	9		23	17(4)
2^+	1	0.58	25	9		20	23(6)
Σ						226	259(39)

in the left panel of Fig. 5.13, where the solid line represents a fit to the experimental spectrum. The different grey lines correspond to a Monte Carlo simulation of the individual decay channels. The gamma-rays facilitated the experimental determination of partial cross-sections that are summarised in Table 5.1. The calculations shown in this table correspond to single-particle cross sections in the spectator-core eikonal three-body model. They are given separately for stripping and diffractive breakup. The theoretical cross-section for a given ^{10}Be core final state and the j value of the removed nucleon is assumed to be the product of a spectroscopic factor (C^2S) [112] and a single-particle cross section, which is the sum of the different contributions mentioned above. This theoretical cross section is then compared with the experimental values, allowing us to test the picture provided by the reaction mechanism description and the nuclear structure (spectroscopic factors calculated within the shell model). Data recorded in Table 5.1 show a quite good agreement between the experimental results and theoretical calculations. This result also corroborates a dominance of an s-wave single particle configuration for the ground-state.

With this experimental setup, it was possible to discriminate the ground-state from the other excited states for the ^{10}Be fragment momentum distribution. The results are shown in the right panel of Fig. 5.13, together with calculations assuming a knockout reaction from s, p and d neutrons. Here we see that the narrow momentum distribution (FWHM = 47.7(6) MeV/c), associated with the ^{10}Be g.s., is only compatible with the case of nucleon removal from a 1s state. This experiment was very successful in determining the ground state structure of ^{11}Be, quantifying the admixture of the ^{10}Be excited core to it. It provided a good understanding of the reaction mechanism and structure of the nuclei involved.

- One-proton halo ^{8}B

  ^{8}B with one bound state and a one-proton separation energy of 137 keV, is the only known nucleus with a proton halo structure in its ground state. Experimental evidence for it was seen in earlier measurements of a large one-proton removal cross section of 98 ± 6 mb (on carbon) and a narrow longitudinal momentum distribution of 93 ± 5 MeV/c [113–115].

  Because it is an $A = 8$ nucleus, reactions involving ^{8}B are important to understand how stellar nucleosynthesis bridges the $A = 8$ mass gap. In addition, the astrophysical interest in ^{8}B stems from its key role in the production of high-energy solar neutrinos [116]. The need for accuracy in the high-energy solar neutrinos production has not diminished after the reports on neutrino oscillations [117]. Indeed, the proton capture rate of ^{7}Be strongly depends on the structure of ^{8}B.

  When describing ^{8}B as a one-proton halo system, one should keep in mind that the ^{7}Be core is itself a weakly bound system, which can be considered as a two-body system (^{4}He + ^{3}He). The ^{7}Be $3/2^-$ ground state is bound by 1.587 MeV, and the only bound state below the $\alpha + ^3$He threshold is the $1/2^-$ state at 429 keV excitation energy. If ^{8}B is treated as a two-body system, there are three possible ways to couple a proton to the ^{7}Be core: the last proton in ^{8}B can be in either a $p_{3/2}$ or a $p_{1/2}$ state, and the possible ground state configurations of $^8\mathrm{B}(I^\pi = 2^+)$ thus are:

  (a) $\psi(^7\mathrm{Be}(3/2^-)) \otimes \psi(p(3/2^-))$
  (b) $\psi(^7\mathrm{Be}(3/2^-)) \otimes \psi(p(1/2^-))$
  (c) $\psi(^7\mathrm{Be}(1/2^-)) \otimes \psi(p(3/2^-))$

  An experiment was performed at the FRS (GSI) [46, 47] with a ^{8}B beam at 936 MeV/nucleon, produced by nuclear fragmentation of a ^{12}C primary beam. This ^{8}B beam impinged on a C target located at the intermediate focal plane of the FRS. Fragment longitudinal momentum distributions after proton knockout and the cross-sections of the processes were determined in the experiment. An array of NaI(Tl) detectors, located close to the knockout target and covering the forward direction, allowed the coincident measurement of the 429 keV γ rays.

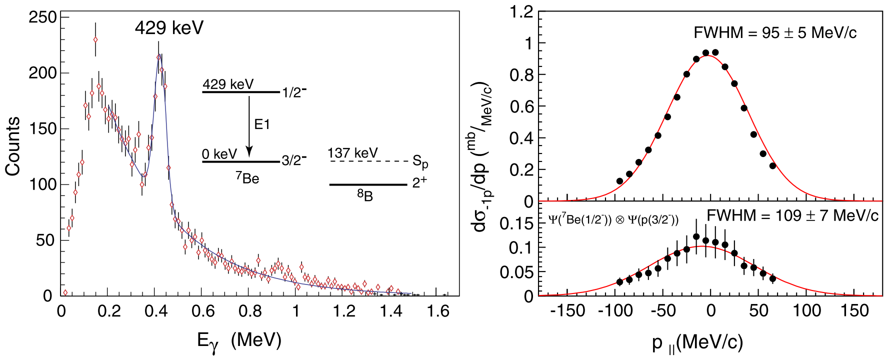

Fig. 5.14 *Left*: Energy spectrum of γ rays after Doppler correction in coincidence with ^{7}Be fragments after one-proton removal reactions of ^{8}B in a carbon target. *Right*: (*top*) Inclusive and (*bottom*) exclusive $p_\parallel$ momentum distribution of ^{7}Be core-fragments emerging from the ^{12}C(^{8}B, ^{7}Be + γ)X one-proton knockout. Exclusive data refer to contributions in coincidence with the 429 keV state in ^{7}Be. In both cases, the *full curve* represents the theoretical calculation folded with the experimental resolution and scaled to match the amplitude of the experimental spectrum [46, 47]

Table 5.2 Comparison between theoretical and experimental results for inclusive (total) and excited (in coincidence with the γ-peak at 429 keV in ^{7}Be) one-proton removal cross sections and $p_\parallel$ (FWHM) after one proton removal of ^{8}B. The theoretical widths in this table include the experimental resolution

	$\sigma_{-1\text{p}}$ (mb) exp.	$\sigma_{-1\text{p}}$ (mb) theo.	$p_\parallel$ (MeV/c) exp.	$p_\parallel$ (MeV/c) theo.
Total	94 ± 9	82	95 ± 5	99
Excited	12 ± 3	11.5	109 ± 7	130

Tracking detectors located at the final focal plane determined the momentum distribution of the ^{7}Be fragments after one-proton removal process of ^{8}B. This coincidence measurement provided direct information about the contribution from configuration (c) to the ^{8}B ground state wave function.

The gamma-rays recorded in the experiment are presented in the left panel of Fig. 5.14. A summary of the experimental results achieved is also shown in Table 5.2. The theoretical values were obtained using the eikonal approximation with a three body model (^{4}He + ^{3}He + t) to describe the ^{8}B wave function. The gamma coincidence also allowed to discriminate the fragment longitudinal distribution involving configuration (c) from the others. In this case the removed protons are always in a p state as shown in the right panel of Fig. 5.14, and almost no difference in the fragment momentum distribution width is observed.

The ratio of the cross section of ^{7}Be in its excited state to the total cross section is found to be 13 ± 3 % which is in excellent agreement with the theoretical value of 14 %. This indicates that the $\psi(^7\text{Be}(1/2^-)) \otimes \psi(p(3/2^-))$ component in the ^{8}B ground state wave function has a significant weight of about 16 %. The ratio

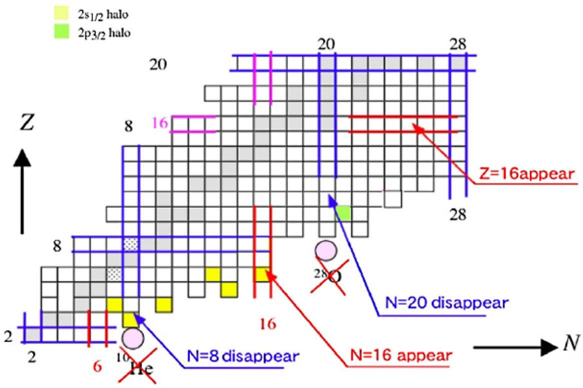

Fig. 5.15 The nuclear chart showing the region of light nuclei where different shell changes have been identified following empirical systematics of nuclear properties [120, 121]. Figure extracted from [120]

between the experimental and theoretical cross section indicates how realistic is the "prescription" used in the model. This will be explained later in Sect. 5.2.3.5.

5.2.3.2 Excursion to Nuclear Shells

Since the early work of Goeppert-Mayer and Jensen [12, 13, 118, 119], a description of the nucleus as formed by nucleons under the action of a central potential plus a spin-orbit interaction was accepted. The energy ordering of nucleons in nuclei showed important gaps at given nucleon numbers, pointing to the existence of "closed shells", where the maximum occupancy of the shell is reached. These nucleon numbers are known as "magic numbers" and provide extra stability to the nuclear system. The finding of magic numbers has been later confirmed by the presence of discontinuities associated with them, and observed in the systematic study of several nuclear properties, such as the evolution of the B(E2) strength.

This idea has been, and still is today, the robust pillar on which the shell model stands to explain the nuclear properties. The important technological improvements, achieved during the 60 years elapsed, have brought the opportunity of increasing the number of nuclei accessible for experiments.

Present nuclear studies concentrate on the investigation of species far away from the β-stability valley, characterized by the imbalanced number of protons and neutrons they own. The manifestation of new phenomena such as the nuclear halo discussed in Sect. 5.2.3.1 has been observed in some nuclei. As a general feature, unexpected structural properties result from a rearrangement of the nuclear orbitals, manifested in some of the exotic species studied.

This rearrangement has resulted in a modification of the traditional magic numbers [120] that we will address in this section and which is summarized in Fig. 5.15. A detailed review of these topics can be found in [120, 121].

To understand the importance of these modifications it is necessary to establish the connection between possible deviations from the expected picture, based on our knowledge of stable nuclei, and a more microscopical interpretation. From this point of view, a major contribution of isospin dependent terms in the nucleon-nucleon interaction could be reasonable and is today accepted [122–125] (and references therein). The need to include terms in the nuclear interaction corresponding to three-nucleon force contributions [75, 126, 127] has become obvious.

We will highlight some nucleon-knockout experiments that have contributed to the study of shell evolution close to the nuclear driplines. Again, the discussion will be restricted to the lower part of the nuclear chart.

Several experimental findings pointed to the vanishing of $N = 8$ magic number. Many experiments have addressed the study of ^{11}Li, starting with the interaction cross-section measurements [23] and followed by neutron knockout experiments [25, 128] and transfer reaction studies [129]. In a traditional shell-model picture ^{11}Li would have the valence neutron in the $1p_{1/2}$ orbital, but measurements evidenced a mixing probability of neutrons in the $1p_{1/2}$ but also in the $2s_{1/2}$ orbital. In the same direction, the study of the one-neutron knockout from ^{11}Be [111] (see Sect. 5.2.3.1) showed a major residence of neutrons in the $2s_{1/2}$ orbital. Other experiments, such as neutron transfer [130], Coulomb dissociation [42] and measurements of the magnetic moment [131] yielded similar conclusions: the breakdown of the shell gap at $N = 8$ with the presence of the intruder $2s_{1/2}$ orbital into the p-shell. The other example showed in Sect. 5.2.3.1, the one-proton knockout from ^{8}B [46], was used to explore whether a similar behaviour is present in the $Z = 8$ shell. In this case, the location of the proton halo in the usual $p_{3/2}$ orbital was confirmed and thus no shell change related.

A very intense experimental activity has concentrated on the $N = 20$ shell region. The oxygen isotopic chain ending at ^{24}O, with the non-observation of ^{28}O and ^{26}O as bound states suggested the vanishing of the $N = 20$ in this region. Many studies have addressed the identification and characterization of the so called "island of inversion" formed by nuclei whose ground states exhibit configuration mixing across the $N = 20$ shell. This weakening of the $N = 20$ shell was experimentally supported by the systematic measurements of B(E2) values for different Mg isotopes ($^{30–32}$Mg) related with the lowering of the 2^+ excitation energies. Another exhaustive work was that of the one-neutron knockout of ^{28}Ne [132] which will be described later in this lecture (see Sect. 5.2.3.3). The conclusion of this work identified the presence of fp-intruder orbitals in the ground state of ^{28}Ne. Along the same lines, one could also mention the one-neutron knockout of ^{30}Mg and ^{32}Mg [133], where the ground states show mixing configurations of $1f_{7/2}$ (dominating) and $2p_{3/2}$ orbitals and the one-neutron knockout of the very n-rich ^{33}Mg [50], which reveals in the ground state a mixing of $1f_{7/2}$, $2p_{3/2}$ and $1d_{3/2}$, with the intruder $2p_{3/2}$ contribution being quite significant.

Complementary manifestation of this shell evolution is the appearance of new shell gaps. A nice example is the observed shift of the $N = 20$ shell towards $N = 16$ for the case of light n-rich nuclei. The one-neutron knockout from the last bound oxygen isotope ^{24}O [49] was studied at the FRS. The measured inclusive momentum distribution (see Fig. 5.16) showed a clear evidence of $2s_{1/2}$ neutron occupation. The experimental determination of the associated spectroscopic factor is 1.74(19) and is compared in Table 5.3 with theoretical spectroscopic factors evaluated within the shell model using different effective interactions (SDPF-M and USDB). This large

Table 5.3 Spectroscopic factors for the $2s_{1/2}$ orbital following one-neutron removal from ^{24}O. The experimental value is compared with those determined using the SDPF-M and the USDB interactions. The experimental spectroscopic factor is obtained from a best fit of the ^{23}O momentum distribution (see Fig. 5.16)

	SDPF-M C^2S	USDB C^2S	ExpS C^2S
$1/2_{g.s.}$	1.769	1.810	1.74 (19)

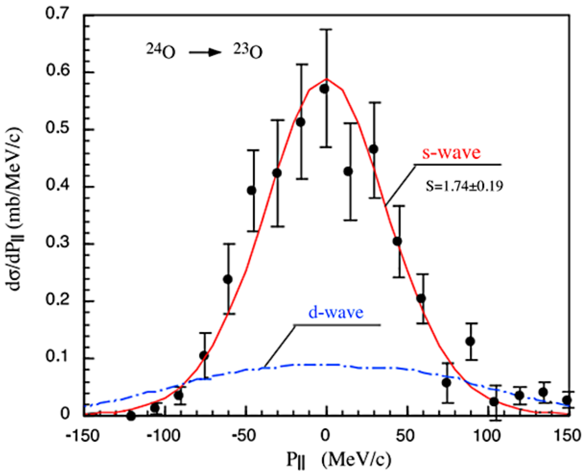

Fig. 5.16 Longitudinal momentum distribution after one-neutron removal from ^{24}O. The *solid curves* correspond to the eikonal model for neutron knockout from $2s_{1/2}$ *in red*, and $1d_{5/2}$ *in blue* [49]. Figure extracted from [49]

spectroscopic factor implies a strong concentration of the single-particle strength of the valence neutron in the $2s_{1/2}$ orbital, which indicates the existence of a large gap between the $2s_{1/2}$ and the $1d_{3/2}$ orbitals, consistent with a new shell gap at $N = 16$. This reveals ^{24}O as a new doubly closed shell nucleus.

The experimental determination of the shell gap (≈4.8 MeV) has been possible from the 2^+ lowest resonance energy in ^{24}O observed in the one-proton removal from ^{26}F to $^{23}\text{O} + n$ [134]. This result was also confirmed by Ref. [135], measuring unbound excited states of ^{24}O via proton inelastic scattering ($^{24}\text{O}(p, p')^{23}\text{O} + n$ reaction) in inverse kinematics at a beam energy of 62 MeV/nucleon at RIPS. We mention also interesting results on ^{22}C two-neutron knockout [41] performed at RIBF, that found a large spectroscopic factor of 1.403 for the $2s_{1/2}$ component in order to explain the narrow momentum distribution measured which further supports the $N = 16$ as a new magic number.

5.2.3.3 Benchmark of Nuclear Structure Models

The inherent complexity of quantifying structural properties (i.e.: the determination of C^2S) from the analysis of nucleon-removal reactions increases significantly as

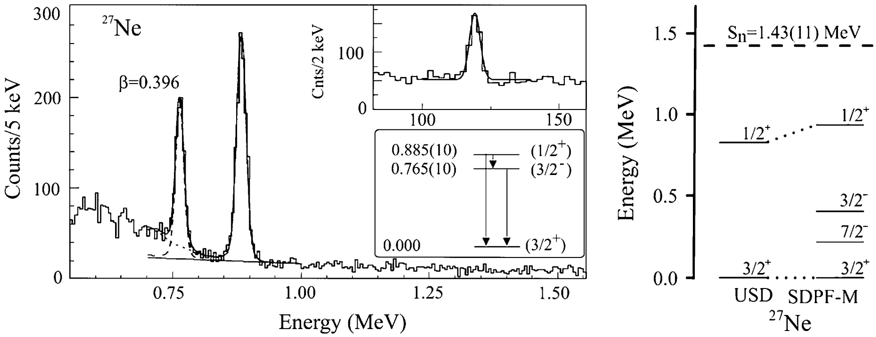

Fig. 5.17 *Left*: Doppler-reconstructed gamma-ray energy spectra for single neutron removal from ^{28}Ne. *Right*: Bound states predicted for ^{27}Ne by USD and SDPF-M calculations [132]. Figure extracted from [132]

nuclei closer to the β-stability are addressed, involving the knockout of more bound nucleons and increasing the amount of available final states.

However, it is important to stress that even in these complex cases the nucleon-knockout technique has proven to be very useful in providing structural information. An example is the neutron knockout of ^{28}Ne [132]. This experiment was performed at NSCL with a secondary beam of about 80 MeV/nucleon using SeGA [136],[21] a segmented Ge detector covering an angular range from 24° to 147°. Figure 5.17, left, shows three gamma-rays at 0.119 (inset Fig. 5.17 left), 0.765, and 0.885 MeV, recorded from the ^{27}Ne de-excitation. The 0.119 and 0.765 MeV gamma-rays were found to be in coincidence, suggesting that only two excited states were populated, as shown in the inset of this figure, and confirming the previous work [137].

The exclusive longitudinal momentum distributions were obtained by applying the coincidence method. Both ^{27}Ne excited states were associated with removed neutrons with $l = 0$ or $l = 1$ but the large experimental errors did not allow a definitive assignment. The momentum distribution of ^{27}Ne ground sate was significantly broader, but quantitative interpretation was not possible.

Figure 5.17, right, shows two different shell-model calculations for ^{27}Ne. Both interactions give very different predictions for the neutron-rich Ne isotopes, which are located in a transitional region between $N = 16$ and $N = 20$ (discussed in Sect. 5.2.3.2). Conventional calculations performed with the Universal SD (USD) interaction with a limited configuration space, do not allow for intruder configurations across the $N = 20$ gap, and thus fail to reproduce shell-breaking effects near $N = 20$. SDPF-M calculations indicate that intruder configurations are important for ^{27}Ne ($N = 17$), even in the low-energy part of the level scheme. Conversely, SDPF-M predictions in this transitional region also compare well with known level structures and electromagnetic moments.

[21] Segmented germanium array.

What is interesting here is that the ^{27}Ne measured gamma rays show the presence of low-lying states and are consistent with the SDPF-M shell model calculations. This contradicts the USD shell model, which predicts only one bound excited state.

Further analysis in terms of exclusive cross-sections was also carried out by the authors, who calculated single particle cross sections in the three-body reaction model [138]. The ratio of experimental and single particle cross sections made it possible to determine experimental spectroscopic factors. Spectroscopic factors from the SDPF-M model were not yet available, providing only an upper limit, which was however in quite good agreement with the experimental spectroscopic factors.

This experiment reported direct evidence of population of the $3/2^-$ intruder state in ^{27}Ne in the knockout of a single neutron from the ground state of ^{28}Ne. There are two important implications to this experimental finding; first, that this low-lying negative parity state is consistent with a narrower shell gap for exotic nuclei with $Z \ll N$ and $N \approx 20$; second, it clearly favoured Monte Carlo shell-model calculations with the modern SDPF-M interaction that successfully describe neutron-rich nuclei in the vicinity of $N = 20$, where normal and intruder configurations coexist at low excitation energy.

Another example can be found in the study of neutron-rich Ca, Ti and Cr nuclides around $N = 32$–35, where the GXPF1A interaction predicts a new doubly-magic shell closure for the $N = 34$ nucleus ^{54}Ca. This nucleus, can not be reached experimentally yet, but some nuclei in the neighbourhood, like ^{55}Ti [90], could be explored. The one-neutron knockout from ^{56}Ti using the FRS as a two-stage magnetic spectrometer and the Miniball [89] array for gamma-ray detection allowed the determination of inclusive and exclusive cross sections and longitudinal momentum distributions of ^{55}Ti, providing later the determination of the orbital angular momentum of the populated states. The measured data allowed for the first time to establish the ground state of ^{55}Ti as $1/2^-$, in agreement with shell model predictions using the GXPF1A (carefully tested in the pf-shell region [91, 139]).

The same interaction showed a reasonable agreement, reproducing the inclusive measurements of one-neutron knockout of $^{51-55}$Sc [54] for nucleons removed from p orbitals. However, an important mismatch between the experimental and theoretical cross-section was observed for the case of neutrons removed from f orbitals. The authors explained the discrepancy suggesting a migration of the spectroscopic strength of neutrons (in $f_{7/2}$) across the $N = 28$ shell gap. Indeed, this shell reduction has been recently predicted in Ca isotones, by realistic NN interactions plus three body interactions [127], highlighting possible shortcomings in the GXPF1 interaction.

Consequently, these examples do not only demonstrate the general importance of direct reactions and particularly nucleon-knockout for the study of exotic nuclei, but can definitively be considered as excellent benchmark experiments for the predictive power of large-scale shell-model calculations and an important tool to improve them.

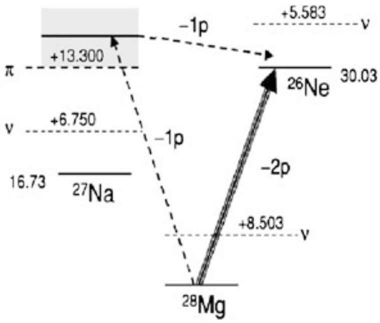

Fig. 5.18 Energy diagram of the neutron-rich $N = 16$ isotones (^{28}Mg, ^{27}Na, and ^{26}Ne), illustrating that direct population of the bound states of ^{26}Ne from ^{28}Mg is favoured over the two-step process of one-proton removal to excited ^{27}Na followed by proton evaporation [140]. Figure extracted from [140]

5.2.3.4 Two Nucleon Removal

The panorama of "direct reactions" induced by exotic beams was enlarged by Bazin and collaborators [28], who suggested the two-proton removal of very neutron-rich nuclei as a single step direct reaction.

It is based on the idea that the competing two-step process of a first proton-knockout followed by a proton evaporation is strongly suppressed in comparison with the neutron evaporation from the neutron-rich intermediate state, which is shown in Fig. 5.18 (extracted from [140]). This pioneering work was followed by a rather intense activity in both experimental [3, 28–33] and theoretical [140, 141] aspects (see also [1, 3]).

The inclusive cross-section of the two-nucleon knockout process is significantly smaller than the corresponding one-nucleon process, reaching maximum values of only a few mb. Even though the cross-sections are small, interesting results have been obtained. They refer, as in the case of single-nucleon knockout, to the momentum distributions of the emerging fragment and the associated cross-sections (both inclusive and exclusive).

The first experiment [28] performed at NSCL, concentrated on the study of two-proton knockout from neutron-rich nuclei (^{28,30}Mg and ^{34}Si). The *A-2* heavy residues were detected with the A1900/S800 [84] spectrograph and the SeGA [136] array allowed the coincident detection of the γ-fragment de-excitation. The interpretation of these data pointed to the direct character of the process. This early work, which included a simplified reaction model where the two removed nucleons were uncorrelated and diffractive processes were completely neglected, provided a rather good agreement. Following experiments proved the validity of the method when applied to the two-neutron knockout of neutron-deficient species, namely ^{34}Ar, ^{30}S and ^{26}Si [29]. Similarly to the case presented above, the obtained cross-sections were consistent with direct reaction mechanisms. Cross-sections to individual excited states were measured using particle-γ coincidences with an identical experimental setup to Ref. [28]. In this work, the reaction mechanism description was improved and included ingredients of eikonal reaction theory and correlated many-body wave functions from shell-model calculations. In this model, several reaction mechanisms are considered to participate in the one-step two-nucleon removal: (a) the inelastic removal of both nucleons, (b) the elastic removal of one of them

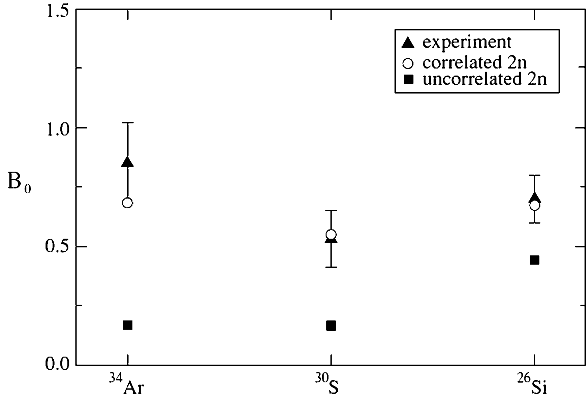

Fig. 5.19 Cross-sections for the ground state (*triangles*) in the two-neutron knockout reaction [29], compared with the corresponding theoretical cross-section [141] for correlated (*circle*) and uncorrelated (*squares*) neutrons (figure extracted from [29])

and the inelastic removal of the second and (c) the elastic removal of both nucleons. With these considerations, the cross-section of the two-nucleon removal process is expressed as (ignoring the Coulomb contribution):

$$\sigma = \sigma_{strip} + \sigma_{strip\text{-}diff} + \sigma_{diff}, \tag{5.8}$$

where σ_{strip} and σ_{diff} correspond to events where both nucleons are either inelastically or elastically scattered, and $\sigma_{strip\text{-}diff}$ corresponds to one nucleon interacting inelastically, while the other scatters elastically (details on the reaction model can be found in [140, 141]). The first two processes involve energy transfer to the target nucleus. Typically, and for the case of removal of well-bound nucleons, the diffraction mechanisms (options (b) and (c) in previous paragraph) amount for at least 40 % of the cross-section.

From the comparison of the cross-sections for the ground-state state with the theoretical estimations it was concluded that the presence of correlations between the knockout nucleons is needed in order to reproduce the experimental data (see Fig. 5.19).

Other experiments followed, extending the study to other nuclear chart regions (i.e.: $N = 20$ [31], $N = 28$ [30, 32]). The possibility of extracting structural information from the exclusive momentum distributions in a similar way as the one-nucleon knockout process was also reconsidered, and a reformulation of the theoretical calculation adapted to the two-nucleon removal case was proposed [142].

Sophistications introduced later consisted of simultaneous identification of the residual heavy fragment, the removed proton and other light charged particles after the two-proton removal reaction from ^{28}Mg projectile [143]. The experiment was again performed at NSCL, the heavy fragment was detected by the A1900/S800 [84] spectrograph and the protons and other light charged particles were detected with the HiRA [97] array. These data complement the previous work of Ref. [28], detecting the coincidence between the heavy residue and its γ de-excitation. In this new case triple coincident events were recorded, consisting of two charged particles detected in HiRA and the ^{26}Ne fragments in the spectrograph. As mentioned above, besides protons HiRA was also able to record other light charged particles like deuterons,

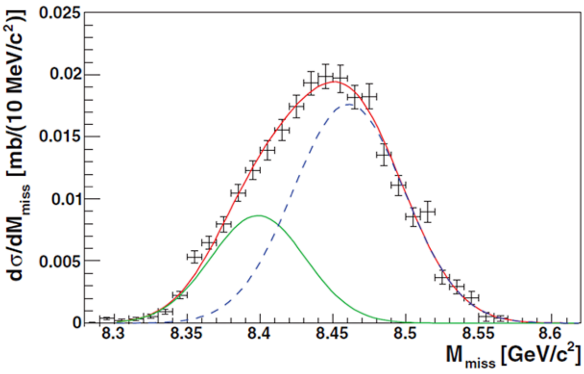

Fig. 5.20 Two-proton removal from ^{28}Mg. Missing-mass spectrum for events where two protons were detected in coincidence with the ^{26}Ne residue. The spectrum was fitted with two Gaussian peaks. The lower peak, at the target mass, is due to the diffraction mechanism (*green*, *solid line*), and the larger peak is attributed to events where at least one proton was removed in an inelastic collision with the target (figure extracted from [143])

tritons or α's, coming from inelastic reactions of the removed protons with target nucleons. The individual contribution of the three removal mechanisms was deduced from the missing-mass calculated for each triple-reconstructed event. Figure 5.20 shows the missing-mass spectrum for events where two protons were detected in coincidence with the ^{26}Ne residue. The experimental results obtained are consistent with the expectations of the eikonal theory described in [141].

With this scenario two-nucleon removal reactions are nowadays fully accepted as spectroscopic tools. In the case of direct knockout of "well-bound" nucleons, the associated cross-sections and *A-2* fragment momentum distributions are considered as a source of information which enables to probe structural changes. They also provide information of the existence of correlations at the nuclear surface.

To date, the knockout of two-weakly bound nucleons has not been widely explored. Experimental conditions do not favour the direct process and the two step reaction mechanism is dominant in this case. Simpson and Tostevin [144] made a careful analysis of this scenario, interpreting two-neutron removal from neutron-rich carbon isotopes ($^{15–19}$C). This work determined the contribution of the single-step process to the measured cross-sections being only 10 % of the total cross-section.

Other experiments [41] have been performed at RIBF (Japan) employing unprecedented intensities for exotic secondary beams of ^{19,20,22}C at around 240 MeV/nucleon. Narrow momentum distributions were observed after one-neutron knockout of ^{19,20}C and two-neutron removal of ^{22}C, whereas the two-neutron removal of ^{20}C yielded much broader distributions. These results together with the associated cross-sections were interpreted in the case of single-nucleon knockout with help of an eikonal reaction model. The obtained results agree quite nicely with the general systematics and will be discussed in the next section.

For the interpretation of two-neutron removal cross sections, the case of one-neutron removal through unbound intermediate states followed by decay to a bound state as well as the direct two-neutron removal case were considered. A clear dominance for the first mechanism, with a direct contribution of around 8 % only and thus consistent with the early work of Simpson et al. [144] was obtained. Unfortunately the setup being used did not allow for exclusive measurements and the firm empirical confirmation of this estimation has still to wait for future experiments.

5.2.3.5 The Quest of Spectroscopic Factors

In previous sections we have discussed the ability of knockout reactions to determine the nuclear structure of rare isotopes. It has been also discussed that in order to reach this goal, it is necessary to compare the experimental observables with detailed calculations that require two main ingredients: a structure model and a proper description of the reaction mechanism (see Sect. 5.2.1).

Section 5.2.3.1 recounts in detail how knockout reactions are able to determine the nuclear structure of weakly bound halo states in which the proton (neutron) single-particle picture, the basis of the shell-model, is very realistic. But what happens when the knockout involves deeply bound states? In this case the picture provided by the shell model could be far from complete. Presently, truncated model-space effective interactions are employed and these are known to include only partially correlation effects that could be of importance in the case of deeply bound states. Indeed, the importance of these correlation effects can be evaluated from the determination of the single-particle spectroscopic strengths.

An important body of strength functions was obtained for the case of stable nuclei from electron-induced quasi-free scattering $(e, e'p)$ obtained some decades ago. In these cases, it has been observed that the spectroscopic strength of valence protons (R_s)[22] exhibit a value of ≈0.6–0.7 [5], with R_s being the ratio between the experimental and theoretical cross-section. It will be of interest to extend the use of this technique to gain information on exotic nuclei. This could be achieved in the future with eA colliders, as the one foreseen in ELISe/FAIR [145] experiment. In the mean time, one can utilize other suitable direct reactions such as transfer and hadron knockout.

In the particular case of knockout reactions, and under the assumption of the correctness of the reaction description provided by the eikonal model, R_s (deduced by Eq. (5.6)) can be taken as a quantification of the pertinence of the pure single-particle description. The closer this value is to unity the more realistic the single-particle picture and so the effect of correlations between nucleons is less significant.

If we now come back to the first results of single-nucleon knockout of neutron and proton halo states presented in Sect. 5.2.3.1 and evaluate the corresponding spectroscopic strength we will obtain $R_s \geq 0.8$, significantly larger than the values recorded with stable nuclei. The question is now whether this technique can be applied to the study of exotic species in a general manner and what happens when the knockout of very deeply bound nucleons is addressed.

[22] Definition introduced in Eq. (5.7).

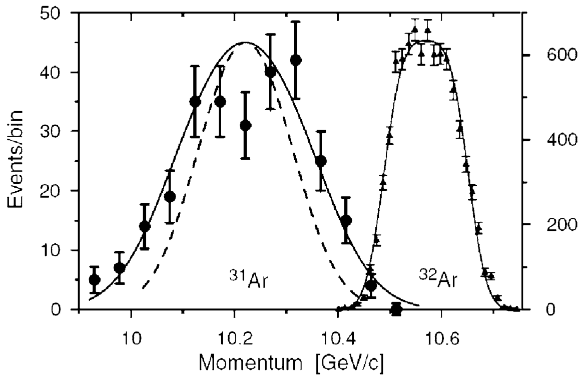

Fig. 5.21 Longitudinal momentum distribution of ^{31}Ar residues after one-neutron knockout reaction, compared with theoretical calculations assuming $l = 0$ (*dashed line*) and $l = 2$ (*solid line*) knocked out neutrons. The unreacted projectile beam ^{32}Ar fitted with a rectangular distribution folded with a Gaussian resolution function is also shown [146] (figure extracted from [146])

An instructive example will be to explore an extreme case such as the experimental study of ^{32}Ar [146] via one-neutron knockout at 61 MeV/nucleon. This nucleus is probably the most bound neutron-removal case investigated so far with this technique, which leads to the proton-dripline nucleus ^{31}Ar. This nucleus, with a $5/2^{+}$ ground state is peculiar because it has no bound excited states. A direct measurement of the core-fragment provides exclusive information without need of gamma coincidence.

From the experimental point of view there is an important difference between this experiment and all the others previously discussed. The S800 spectrograph was operated in "focus mode" with larger acceptance but lower intrinsic momentum resolution, as shown in Fig. 5.21. The theoretical momentum distributions depicted in this figure were calculated using the black-disk model [1] and folded with the measured response of the apparatus. This spectrum clearly associates the reaction with a $l = 2$ knockout neutron, confirming the spin and parity assignment for the ^{31}Ar ground state of $5/2^{+}$. Comparison of the experimental cross section 10.4(13) mb with the theoretical one yields a surprisingly low quenching factor of $R_s = 0.24(3)$. The authors of that work compared this case with ^{22}O, which has the same neutron number $N = 14$ and $Z = 8$ protons, and considered as almost doubly magic nucleus. The quenching factor, obtained in this case is 0.70(6) (using an average of two different experimental results [35, 36, 48] as experimental cross section), which is well above the result obtained for ^{32}Ar. The authors suggested that this very strong quenching is an indication of nuclear structure effects, reflecting correlations linked to the high neutron separation energies (22.0 MeV) in this very asymmetric nuclear system.

Other extremely asymmetric neutron-deficient systems were also explored (^{28}S and ^{24}Si) via one-proton and one-neutron knockout. This work presented in Ref. [147] is very interesting since it allows to explore in the same nuclei both

Table 5.4 Partial cross sections (mb) to all final states I^π after one-neutron and one-proton knockout from ^{28}S and ^{24}Si. Different contributions of theoretical single-particle cross sections in the eikonal model are reported. The sum multiplied by the spectroscopic factor is compared with the experimental values [147]

Fragment	I^π	C^2S	σ_{sp}^{knock}	σ_{sp}^{diff}	σ^{theo}	σ^{expt}	R_s
Projectile ^{24}Si							
$^{23}Al_{g.s.}$	$5/2^+$	3.42	17.56	5.18	84.68	67.3(35)	0.79(4)
$^{23}Si_{g.s.}$	$5/2^+$	1.71	10.96	2.47	25.01	9.9(10)	0.39(4)
Projectile ^{28}S							
$^{27}P_{g.s.}$	$1/2^+$	0.832	20.73	7.84	25.56	31(3)	
$^{27}P_{1.1\ MeV}$	$3/2^+$	0.82	14.61	4.40	16.75	6.8(11)	
$^{27}P_{incl.}$					42.32	38(3)	0.90(7)
$^{27}S_{g.s.}$	$5/2^+$	3.136	8.99	2.10	37.40		
$^{27}S_{e.s.}$	$3/2^+$	0.119	8.72	2.03	1.37		
$^{27}S_{incl.}$					38.77	11.9(12)	0.31(3)

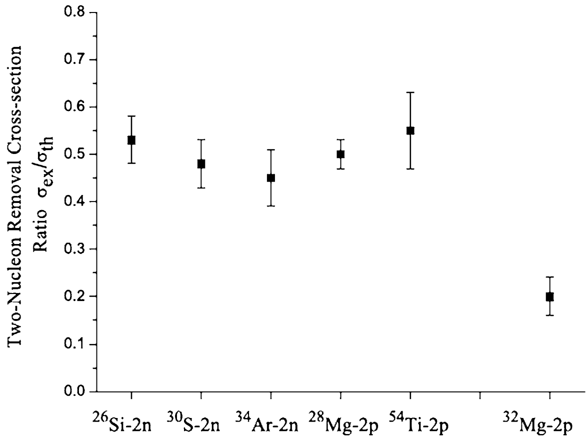

Fig. 5.22 Reduction factor R_s (defined as the ratio σ_{ex}/σ_{th}) evaluated for two-nucleon knockout cross-sections. Note that inclusive and exclusive data are included in the figure, see [31] for details

single-particle strengths associated with weakly bound nucleons (protons in the one-proton knockout case) and strongly bound nucleons (neutrons in the one-neutron case). The R_s values obtained are recorded in Table 5.4. Again, we can observe very different values of R_s for the two reaction channels studied.

These experimental results reinforce further the strong reduction observed in single particle strengths of deeply bound nucleons, whereas the reduction factor is close to unity for the case of knockout of weakly bound nucleons. A similar analysis performed for the two-nucleon removal cases discussed in Sect. 5.2.3.4, yields very similar results [31] (see Fig. 5.22), with R_s around 0.5 except for the ^{32}Mg case.

It is illustrative to analyse the systematic comparison performed by Gade and collaborators [147] (see Fig. 5.23), in which they represent an important collection

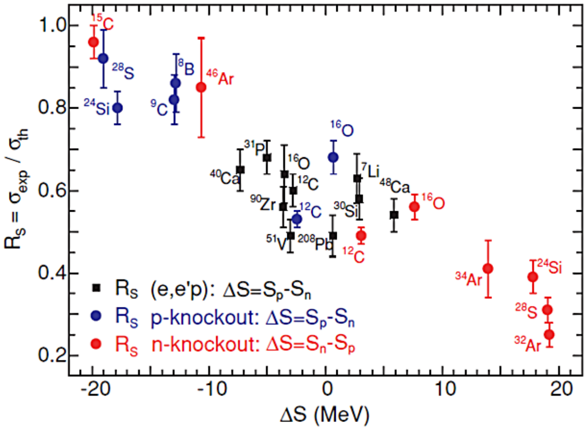

Fig. 5.23 Summary of quenching or empirical reduction factors obtained for spectroscopic factors evaluated from knockout reactions [147] (figure extracted from [147])

of the measured R_s reduction factors as a function of the difference in separation energies of the nuclei considered (ΔS). The quantity ΔS measures the asymmetry of the Fermi surface for each nuclei.[23] The following definitions $\Delta S = S_p - S_n$ and $\Delta S = S_n - S_p$ stand for the case of proton and neutron knockout respectively. Note that the figure also includes data from $(e, e'p)$ measurements mentioned earlier [5].

Is interesting to note that the physical occupancies are in general much lower than those suggested by the shell model, however this discrepancy is smaller for loosely bound nuclei (≈0.85 left top corner in Fig. 5.23). Cases corresponding to proton-removal from relative symmetric nuclei, with values ranging from 0.5 to 0.6, are in agreement with the findings obtained earlier with quasi-free "proton knock-out" $(e, e'p)$ reactions that addressed stable nuclei and with $\Delta S \approx 0$. Knockout of deeply-bound nucleons as the ones represented by the neutron-knockout in near proton-dripline nuclei (right bottom corner in Fig. 5.23) are associated with R_s factors lower than 0.4. Using $(e, e'p)$ [148] as an analogy again, this small reduction factor is interpreted in terms of correlation effects that reveal the incomplete and simplified picture of nuclei provided by effective-interactions used nowadays. To complete the picture, note that Fig. 5.23 contains a mixture of exclusive and inclusive information. In the inclusive knockout cross section the quenching factor R_s is defined as the ratio of the experimental cross section to the sum of the theoretical cross sections to any state lying below the neutron threshold.

In spite of such significant experimental and theoretical progress, the tendency shown in Fig. 5.23 is not fully understood. The determination of absolute spectroscopic factors is a hot topic in the nuclear structure domain. The information gained with nucleon removal reactions induced by radioactive beams is undoubtedly important. The interplay between the nuclear structure and reaction input is necessary in order to extract this information, and the incomplete description of any of these ingredients could be the origin of the strong reduction observed. This interesting topic will be the subject of study in the coming years and there are plans

[23] Difference between the Fermi level for neutrons and protons in a given nucleus.

to extend it with the use of QFS reactions induced by radioactive beams. There is also an ongoing concerted effort to improve the reaction mechanism understanding (Refs. [152, 157]). The evaluation of spectroscopic factors in the medium-mass range coming from ab-initio calculations is expected to shed light on this exciting topic.

5.3 Quasi-Free Scattering Reactions with Rare Isotope Beams

In this last part of the lecture we will complete the introduction to the Quasi-Free Scattering (QFS) (see Sect. 5.1.1) with recent experiments addressing the study of rare isotopes produced in fragmentation facilities. We will finish reporting on the status and progress of the QFS program with rare exotic isotopes foreseen in future experimental setups such as R^3B [93] at FAIR.

As has been outlined in Sect. 5.2.3.5, further investigations on single-particle properties in rare nuclei, as well as the role of in-medium effects on the NN interactions and the existence of NN correlations, that would complement the work done so far with knockout reactions, are certainly needed.

The use of QFS reactions such as $(p, 2p)$ and (p, pn), induced by high energy proton beams offers very attractive possibilities. QFS reactions are able to excite both valence nucleons and also deep-hole states, giving access to the associated single-particle properties. Compared with the nucleon-knockout cases presented in Sect. 5.3, this reaction channel will not reduce the wave function exploration to the most external regions, thus providing a more complete picture of the structure of the nucleus. Moreover, the detection of both nucleons, the target and the removed nucleon, would provide (together with the gamma de-excitation of the *A-1* fragment) fully exclusive measurements, that in turn could help to characterize the reaction mechanism.

Up to now, we have only referred to QFS experiments performed in direct kinematics, with high energy protons impinging on the nucleus of interest [57]. It is clear that the use of inverse kinematics opens the exciting possibility of exploring nuclear structure for all kind of nuclear species.

A first attempt to this experimental approach took place few years ago at the HIMAC (Heavy Ion Medical Accelerator in Chiba) facility in NIRS (National Institute of Radiological Science in Japan) by Kobayashi and collaborators [149]. Different carbon isotopes ($^{9-16}$C) at 250 A MeV impinged on a solid-hydrogen target. These reactions provided an excellent scenario to get systematic information on weakly- to strongly bound $1p$ valence protons (lower N values) and deeply bound 1s inner shell protons (larger N values). The four-momenta of the two protons measured in a two-proton telescope located at $\pm 39°$ with respect to the beam axis allowed the determination of proton binding energy distributions (B_p)[24] of the different states

[24]Noted S_p in Ref. [149].

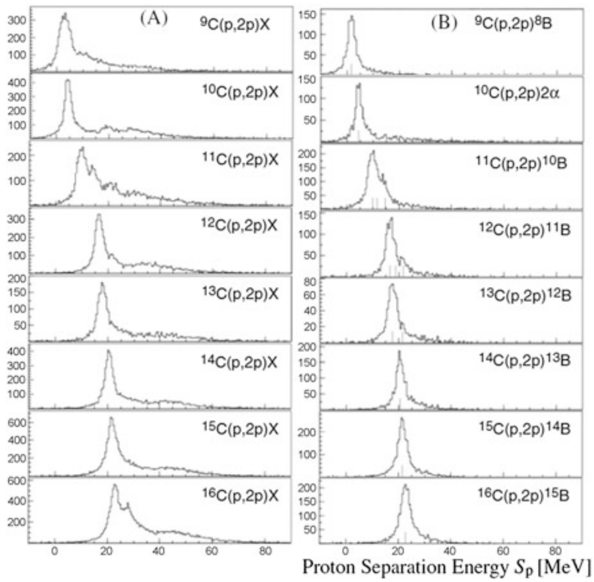

Fig. 5.24 Proton-separation energy distributions (B_p, denoted as S_p in the figure): (**A**) inclusive, (**B**) $^{A-1}$B detected in the forward spectrometer, (**C**) no boron isotopes detected in the forward spectrometer [149] (figure taken from [149])

from which the proton was removed in the projectile (see Fig. 5.24 and (5.9)).

$$B_p = S_p + E^*_{A-1}, \tag{5.9}$$

with S_p in this formula being the minimum energy to separate the last bound proton and E^*_{A-1} the excitation energy of the single particle state relative to the nucleus Fermi level (depending on how deeply bound the removed proton is this magnitude can vary from 0 MeV up to several tens of MeV).

The coincidence with the remaining fragments performed with a forward spectrometer is the responsible of the selection of the different transitions. Those to the ground state (case B in Fig. 5.24), were selected by gating on the $^{A-1}$B (boron) fragments, whereas those to the s-hole states (case C in Fig. 5.24), required the anti-coincidence with B isotopes. The s-holes states are associated with removal of deeply bound protons and are produced with high excitation energies. The high excitation energy allows to open channels decaying via charged particles emission. Those channels, in which the *A-1* fragment does not survive, provide information of the inner region of the projectile wave-function. It is important to mention the good agreement found between the ^{12}C results in this experiment and the one in direct kinematics [57].

In the same experiment, the momentum distributions of protons occupying both p- and s-orbitals could be measured and are presented in Fig. 5.25. In both cases, removal from p (A in the figure) and s-orbitals (B in the figure), one can clearly

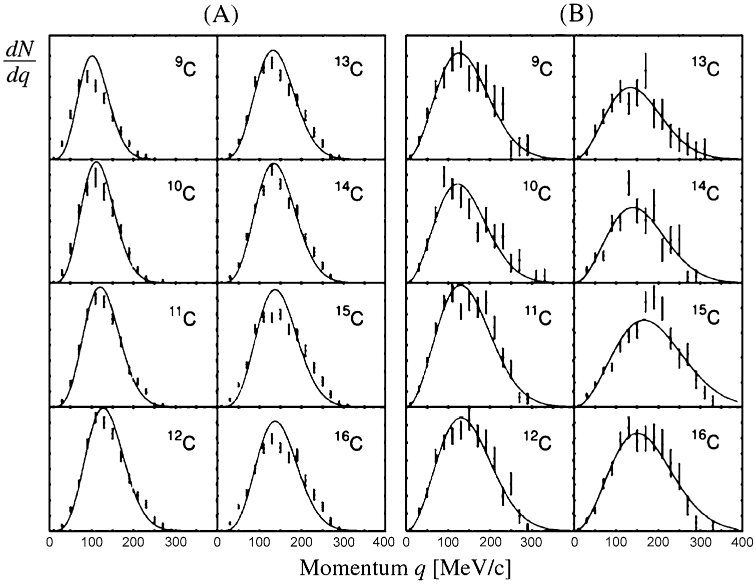

Fig. 5.25 Proton momentum distributions (**A**) for the p-hole states via ^{A}C$(p, 2p)^{A-1}$B$_{gr}$ reaction. (**B**) for the s-hole states via ^{A}C$(p, 2p)\bar{\text{B}}$ [149] (figure extracted from [149])

observe narrower distributions for lower masses (where the valence protons are more weakly bound). An accurate determination of the associated spectroscopic factors was not possible in this work but the systematic evaluation of the ratio of $(p$-hole$)_{yield}/(s$-hole$)_{yield}$ shows an increase for the ^{9}C case. This is also interpreted as a indication, analogous to the nucleon knockout case, of large spectroscopic factors associated with subshells for the weakly bound nucleons.

From the theoretical point of view, QFS has traditionally been interpreted in the framework of Distorted Wave Born Impulse (DWBI) approximation [150, 151]. There are new attempts to formulate a model to describe QFS observables based on the eikonal theory as it is shown in Ref. [152]. On the other hand the description of the QFS reaction mechanism on proton targets (free of stripping contributions) is also possible to be addressed with approaches such as the Continuum-Discretised Coupled Channels method (CDCC) [153–155], or even those based on complex solutions of the full Faddeev/AGS equation [156, 157].

5.3.1 Status of the QFS Program with Exotic Rare Isotopes at R^3B

The study of single particle properties of exotic nuclei is an important part of the experimental programme of several future nuclear physics instruments. First exclusive measurements of QFS reactions of rare isotopes on a proton target have been

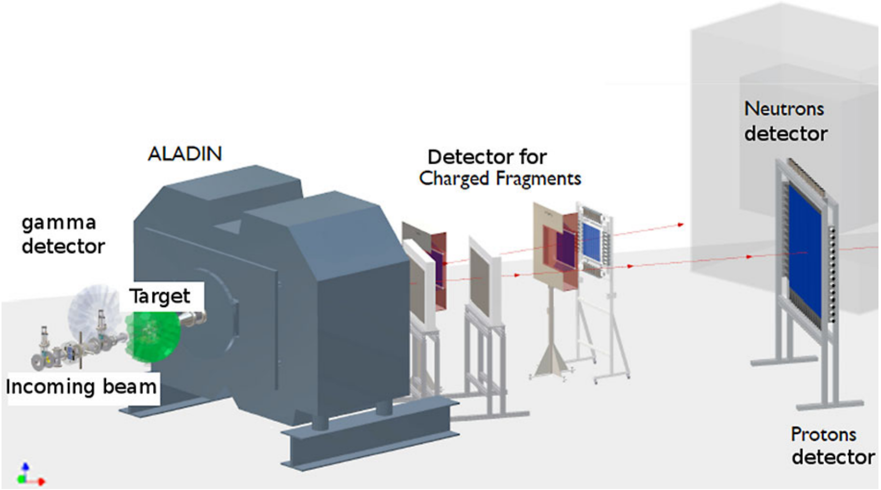

Fig. 5.26 LAND/R^3B setup (precursor of R^3B/FAIR experiment) presently installed at GSI [93]

performed recently at GSI using inverse kinematics with the LAND/R^3B setup (see Fig. 5.26).

The R^3B/NUSTAR [93] collaboration intends to apply this technique using the intense radioactive beams that will be delivered by the SuperFRS/FAIR [158] in inverse kinematics. At energies around 700 MeV/nucleon, both outgoing nucleons have energies in the range where the NN cross section is at a minimum, thus maximizing the transparency of the nucleus and minimizing final state interaction.

The large acceptance and high resolution setup proposed R^3B/FAIR [93] would allow background-free measurements and also for better control of final state interactions.

The well known $^{12}C(p,2p)^{11}B$ reaction has been studied as the best validation of the experimental technique [159, 160] in the existing LAND-R^3B setup (see Fig. 5.26). An incident beam of ^{12}C at 400 A MeV impinged on a CH_2 target. A layer of silicon strip detectors surrounding this target (in a box geometry) and the 4π-calorimeter Crystal Ball. Both detectors allowed the detection of the light reaction products (in the $(p,2p)$ case, two protons emitted back-to-back and with an average angular aperture $\approx 90°$). The rest of fragments are deflected by the large acceptance magnet ALADIN and identified behind it. The neutrons, unaffected by the magnetic field of ALADIN [161], are identified with help of the LAND [162] detector.

Compared with other experiments two novelties are introduced. On the one hand, the proton detection is not limited to a co-planar geometry and on the other, the complete kinematical detection of incident beam and all the fragments emerging from the reaction allows for the first time to record redundant information on the internal nuclear momentum of the removed nucleon, either with the four-momenta determination of the two protons or with the four momenta of the fragment. Figure 5.27 shows the preliminary results [159, 160] of the total excitation energy spectrum of

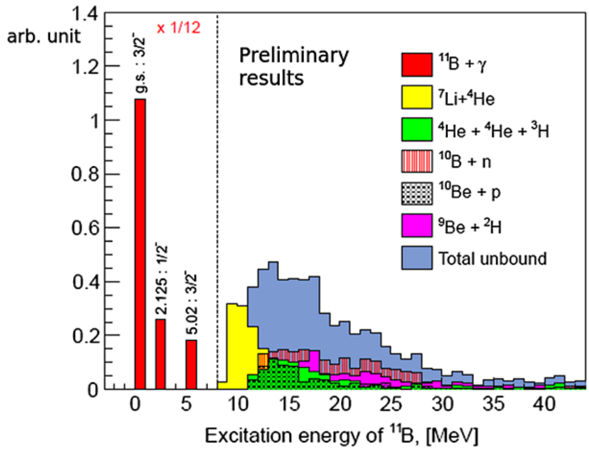

Fig. 5.27 Total excitation energy spectrum of the residual ^{11}B for the ^{12}C$(p,2p)^{11}$B reaction [159, 160]

the residual ^{11}B coming from ^{12}C$(p,2p)^{11}$B reaction that are in good agreement with other data addressing the same reaction [57, 149].

Different experiments[25] studying light neutron-rich nuclei with Z ranging from 4 to 9 produced by fragmentation of a 400 A MeV ^{40}Ar primary beam, and utilizing kinematically complete measurements of reactions at relativistic energies, were also done with the LAND/R^{3}B reaction setup. The physics topics studied comprise the measurement of astrophysical reaction rates relevant for r-process nucleosynthesis using heavy-ion induced electromagnetic excitation and quasi-free knockout reactions to study the evolution of shell and cluster structures close to and beyond the dripline. Unbound (ground and excited) states could be populated and identified in $(p,2p)$ reactions as it is shown in Ref. [163]. The quenching of single-particle strengths in neutron-proton asymmetric nuclei was also addressed by knocking out deeply bound protons and neutrons in $(p,2p)$ and (p,pn) reactions for nuclei with varying neutron-proton asymmetry. The evaluation of this interesting collection of data is presently under analysis and the first results are expected soon.

All these works open a very promising future of new investigations that will one day profit from the high-energy intense radioactive beams at FAIR. They would enable the realization of measurements on exotic nuclei, with the R^{3}B/FAIR experiment overcoming the present experimental limitations. R^{3}B/FAIR [93] will be a versatile reaction setup with high efficiency, acceptance, and resolution for kinematically complete measurements of reactions with high-energy exotic beams. The setup will be located at the focal plane of the high-energy branch of the Super-FRS. A substantial improvement is expected with respect to resolution and an extended detection scheme is foreseen. It will comprise

[25] S393 experiment performed in August 2010, Spokesperson T. Aumann.

– a zero-degree superconducting dipole magnet with a large vertical gap allowing an angular acceptance of ±80 mrad for neutrons and a field up to 5 T able to bend 14° charged fragments for 20 Tm beams.[26]
– a detection setup for light (target-like) recoil particles, formed by a double layer of Si strip detectors. A liquid hydrogen target could be hosted in the inner part of this Si-tracker. The recoil particle detector would provide precise tracking, vertex determination as well as energy and multiplicity measurement with high efficiency and acceptance.
– a new generation spectrometer-calorimeter CALIFA. This detector has to act as spectrometer of low to medium energy γ, being at the same time calorimeter for the target recoil (high energy gammas and light-charged particles). This will be achieved by an extremely segmented detector based on highly performant scintillation crystals (in single [92] or phoswich [164] configuration).[27]
– a dedicated tracking systems for the detection of fragments behind the dipole magnet. For the tracking of light charged particles, i.e. protons, behind the R^3B dipole magnet two identical drift chambers (DHC) are foreseen. Each DCH covers an active area of 100×80 cm^2, thus providing a large enough acceptance behind the magnet to detect decay protons. A large-area scintillating fibre detector is foreseen, for the position measurement of heavy fragments, a few meters behind the magnet. The system is completed by a ToF detector covering the full acceptance of the charged particles and ions produced in relativistic heavy-ion collisions while providing a time-of-flight resolution such that isotopes around the mass 200 can be isotopically resolved.
– a neutron detector NeuLAND featuring a high detection efficiency, a high resolution, and a large multi-neutron-hit resolving power. This is achieved by a highly granular design of plastic scintillators, avoiding insensitive converter material.
– a high-resolution fragment spectrometer that could be constructed in the second phase of the experiment and would substitute the tracking systems for the detection of fragments in those cases demanding high-resolution measurements, where $\Delta p/p$ in the order of 10^{-4} is needed. The proposed solution is based on a spectrometer placed behind the large-acceptance dipole. The spectrometer will be placed at an angle of 18°, which is the maximum bending angle of the dipole (5 Tm field integral) for a beam with magnetic rigidity of 15 Tm, and will be operated as a zero-degree spectrometer.

Lastly we mention another innovative device that will be dedicated to the study of QFS reactions. MINOS (Magic Numbers off Stability) [165], aims to investigate the properties of in-medium NN interactions through the spectroscopy of the most exotic nuclei produced at fragmentation facilities (RIKEN and GSI/FAIR). The project includes the construction of a dedicated and innovative device composed of a thick cryogenic liquid hydrogen target surrounded by a cylindrical time projection

[26]The maximum rigidity provided by the Super-FRS will be 20 Tm.

[27]In a phoswich detectors the energy of the particles is determined from two consecutive energy losses in consecutive detectors.

chamber devoted to determine the reaction vertex by tracking charged particles produced by $(p, 2p)$ or (p, pn) reactions with excellent resolution. MINOS has been built at IRFU, CEA Saclay[28] and will be soon used to perform the first experimental campaign in RIBF/RIKEN.

5.4 Summary and Conclusions

This lecture intended to provide a comprehensive overview of some direct reactions used at high energies to explore the nuclear structure of rare isotopes.

We have presented the interesting implications of using "knockout reactions", emphasizing the experimental and conceptual aspects associated with these kind of experiments and their possible ramifications in the analysis and interpretation of the results.

Halo nuclei, which have a relatively simple and well-known nuclear structure, were used to show the power of the method. Experiments of one-nucleon knockout from halo states provide a very satisfactory description of the reaction mechanism, making it possible to experimentally deduce the structure of the involved nuclei.

Though generally successful, application of the technique to more complex nuclei is not without experimental difficulties that complicate the extraction of quantitative information. Reactions of this kind have been used to measure the physical occupancies (C^2S) associated with the different configurations that define the bound states of the exotic nuclei under study. The experimental spectroscopic factors obtained are generally smaller than those predicted by the large-scale shell model. The existence of these quenching factors has been interpreted in terms of correlation effects pointing out the simplified picture of the nucleus provided by shell model calculations. Deficiencies in the reaction mechanism description could be also behind this effect.

Even though great progress has been made, the situation is not yet clear and the determination of absolute spectroscopic factors with nucleon removal reactions induced by radioactive beams will certainly be a hot topic in the next years. The recent extension of the use of quasi-free scattering reactions in inverse kinematics opens new experimental opportunities. The most important will be the availability of fully exclusive measurements, enabling a better understanding of the reaction mechanism. The information that one can extract about the exotic projectile wave function will not be restricted to the nuclear surface, being possible to extend this exploration to the removal of strongly bound nucleons allowing a deeper study of the role of NN correlations.

Construction and exploitation of new generation facilities (i.e.: NUSTAR/FAIR, BIGRIPS, FRIB), in the near future, will significantly increase the intensity of the available exotic beams. This, together with the development of new specific detection systems (i.e.: R^3B@NUSTAR/FAIR, MINOS ...) will open new perspectives in this field.

[28]Project funded by the European Research Council for the period 2010–2015.

Acknowledgements I would like to thank Dr. B. Pietras for careful reading of the manuscript, valuable comments and multiple English corrections.

References

1. P.G. Hansen, J.A. Tostevin, Direct reactions with exotic nuclei. Annu. Rev. Nucl. Part. Sci. **53**, 219 (2003)
2. T. Aumann, Reactions with fast radioactive beams of neutron-rich nuclei. Eur. Phys. J. A **26**, 441 (2005)
3. A. Gade, T. Glasmacher, In-beam nuclear spectroscopy of bound states with fast exotic ion beams. Prog. Part. Nucl. Phys. **60**, 161 (2008)
4. G. Jacob, Th.A. Maris, Nuclear structure II. Rev. Mod. Phys. **45**, 6 (1973)
5. L. Lapikás, Quasi-elastic electron scattering off nuclei. Nucl. Phys. A **553**, 297 (1993)
6. V.R. Pandharipande, I. Sick, P.K.A. de Witt Hubers, Independent particle motion and correlations in fermion systems. Rev. Mod. Phys. **69**, 981 (1997)
7. G.J. Kramer, H.P. Blok, L. Lapikas, A consistent analysis of $(e,e'p)$ and $(d,{}^3\mathrm{He})$ experiments. Nucl. Phys. A **679**, 267 (2001)
8. M.S. Hussein, K. McVoy, Inclusive projectile fragmentation in the spectator model. Nucl. Phys. A **445**, 124 (1985)
9. C.A. Bertulani, K.W. McVoy, Momentum distributions in reactions with radioactive beams. Phys. Rev. C **46**, 2638 (1992)
10. J.S. Al-Khalili et al., Evaluation of an eikonal model for ^{11}Li-nucleus elastic scattering. Nucl. Phys. A **581**, 331 (1995)
11. D.N. Poenaru, W. Greiner, in Experimental Techniques in Nuclear Physics ed. by W. de Gruyere (Chaps. 10 and 11)
12. M.G. Mayer, On closed shells in nuclei. Phys. Rev. **74**, 235 (1948)
13. O. Haxel, J.H. Jensen, H.E. Suess, On the magic numbers in nuclear structure. Phys. Rev. **75**, 1766 (1949)
14. O. Chamberlain, E. Segrè, Proton-proton collisions within lithium nuclei. Phys. Rev. **87**, 81 (1952)
15. J.B. Cladis, W.N. Hess, B.J. Moyer, Nucleon momentum distributions in deuterium and carbon inferred from proton scattering. Phys. Rev. **87**, 425 (1952)
16. T. Berggren, H. Tryén, Quasi-free scattering. Annu. Rev. Nucl. Sci. **16**, 153 (1966)
17. G. Jacob, Th.A. Maris, Nuclear structure. Rev. Mod. Phys. **38**, 121 (1966)
18. P.K.A. de Witt Huberts, Proton spectral functions and momentum distributions in nuclei from high-resolution $(e,e'p)$ experiments. J. Phys. G **16**, 507 (1990)
19. A.E.L. Dieperink, P.K.A. de Witt Huberts, On high resolution $(e,e'p)$ reactions. Annu. Rev. Nucl. Part. Sci. **40**, 239 (1990)
20. G. van de Steehoven et al., Knockout of $1p$ protons from ^{12}C induced by the $(e,e'p)$ reaction. Nucl. Phys. A **480**, 547 (1988)
21. J. Mougey et al., Quasi-free $(e,e'p)$ scattering on ^{12}C, ^{28}Si, ^{40}Ca and ^{58}Ni. Nucl. Phys. A **262**, 461 (1976)
22. P.G. Hansen, Studies of single-particle structure at and beyond the drip lines. Nucl. Phys. A **682**, 310 (2001)
23. I. Tanihata et al., Measurements of interaction cross sections and nuclear radii in the light p-shell region. Phys. Rev. Lett. **55**, 2676 (1985)
24. I. Tanihata, Research opportunities with accelerated beams of radioactive ions. Nucl. Phys. A **693**, 1 (2001)
25. T. Kobayashi et al., Projectile fragmentation of the extremely neutron-rich nuclei ^{11}Li at 0.79 GeV/nucleon. Phys. Rev. Lett. **60**, 2599 (1988)
26. N.A. Orr et al., Momentum distributions of ^{9}Li fragment following the breakup of ^{11}Li. Phys. Rev. Lett. **69**, 2050 (1992)

27. A. Gade et al., One-neutron knockout in the vicinity of $N = 32$ sub-shell closure: ^{9}Be(^{57}Cr, ^{56}Cr + γ)X. Phys. Rev. C **74**, 047302 (2006)
28. D. Bazin et al., New direct reaction: two-proton knockout from neutron-rich nuclei. Phys. Rev. Lett. **91**, 012501 (2003)
29. K. Yoneda et al., Two-neutron knockout from neutron-deficient ^{34}Ar, ^{30}S, and ^{26}Si. Phys. Rev. C **74**, 021303 (2006)
30. J. Fridmann et al., Shell structure at $N = 28$ near the dripline: spectroscopy of ^{42}Si, ^{43}P, and ^{44}S. Phys. Rev. C **74**, 034313 (2006)
31. P. Fallon et al., Two-proton knockout from ^{32}Mg: intruder amplitudes in ^{30}Ne and implications for the binding of ^{29,31}F. Phys. Rev. C **81**, 041302(R) (2010)
32. D. Santiago-Gonzalez et al., Triple configuration coexistence in ^{44}S. Phys. Rev. C **83**, 061305(R) (2011)
33. A. Gade et al., Cross-shell excitation in two-proton knockout: structure of ^{52}Ca. Phys. Rev. C **74**, 021302 (2006)
34. J.L. Lecouey et al., Single-proton removal reaction study of ^{16}B. Phys. Lett. B **672**, 6 (2009)
35. E. Sauvan et al., One-neutron removal reactions on neutron-rich psd-shell nuclei. Phys. Lett. B **491**, 1 (2000)
36. E. Sauvan et al., One-neutron removal reactions on light neutron-rich nuclei. Phys. Rev. C **69**, 044603 (2004)
37. T. Nakamura et al., Coulomb dissociation of ^{19}C and its halo structure. Phys. Rev. Lett. **83**, 1112 (1999)
38. N. Fukuda et al., Coulomb and nuclear breakup of a halo nucleus ^{11}Be. Phys. Rev. C **70**, 054606 (2004)
39. T. Kubo, In-flight RI beam separator BigRIPS at RIKEN and elsewhere in Japan. Nucl. Methods Phys. Res. B **204**, 97 (2003)
40. T. Ohnishi et al., Identification of new isotopes 125Pd and 126Pd produced by in-flight fission of 345 MeV/nucleon ^{238}U: first results from the RIKEN RI beam factory. J. Phys. Soc. Jpn. **77**, 083201 (2008)
41. N. Kobayashi et al., One- and two-neutron removal reactions from the most neutron-rich carbon isotopes. Phys. Rev. C **86**, 054604 (2012)
42. R. Palit et al., Exclusive measurement of breakup reactions with the one-neutron halo nucleus ^{11}Be. Phys. Rev. C **68**, 034318 (2003)
43. U. Datta-Pramanik et al., Coulomb breakup of the neutron-rich isotopes ^{15}C and ^{17}C. Phys. Lett. B **551**, 63 (2003)
44. C. Nociforo et al., Coulomb breakup of ^{23}O. Phys. Lett. B **605**, 79 (2005)
45. Th. Baumann et al., Longitudinal momentum distributions of ^{16,18}C fragments after one-neutron removal from ^{17,19}C. Phys. Lett. B **439**, 256 (1998)
46. D. Cortina-Gil et al., Experimental evidence for the ^{8}B ground state configuration. Phys. Lett. B **529**, 36 (2002)
47. D. Cortina-Gil et al., Nuclear and Coulomb breakup of ^{8}B. Nucl. Phys. A **720**, 3 (2003)
48. D. Cortina-Gil et al., Shell structure of the near-dripline nucleus ^{23}O. Phys. Rev. Lett. **93**, 062501 (2004)
49. R. Kanungo et al., One-neutron removal measurement reveals ^{24}O as a new doubly magic nucleus. Phys. Rev. Lett. **102**, 152501 (2009)
50. R. Kanungo et al., Structure of ^{33}Mg sheds new light on the $N = 20$ island of inversion. Phys. Lett. B **685**, 253 (2010)
51. C. Rodriguez-Tajes et al., One-neutron knockout from $^{24–28}$Ne isotopes. Phys. Lett. B **687**, 26 (2010)
52. C. Rodriguez-Tajes et al., One-neutron knockout from light neutron-rich nuclei at relativistic energies. Phys. Rev. C **82**, 024305 (2010)
53. C. Rodriguez-Tajes et al., Structure of ^{22}N and the $N = 14$ subshell. Phys. Rev. C **83**, 064313 (2011)
54. S. Schwertel et al., One-neutron knockout from $^{51–55}$Sc. Eur. Phys. J. A **48**, 191 (2012)

55. C. Nociforo et al., One-neutron removal reactions on Al isotopes around the $N = 20$ shell closure. Phys. Rev. C **85**, 044312 (2012)
56. T. Noro et al., A study of nucleon properties in nuclei through $(p, 2p)$ reactions. Nucl. Phys. A **629**, 324 (1998)
57. M. Yosoi et al., Structure of the s-hole state in 11B studied via de 12C$(p, 2p)$11B* reaction. Phys. Lett. B **551**, 255 (2003)
58. R. Subedi et al., Probing cold dense nuclear matter. Science **320**, 1476 (2008)
59. M. Karakoc, A. Banu, C. Bertulani, L. Trache, Coulomb distortion and medium corrections in nucleon-removal reactions. Phys. Rev. C **87**, 024607 (2013)
60. K. Henken, G. Bertsch, H. Esbensen, Breakup reactions of the halo nuclei ^{11}Be and ^{8}B. Phys. Rev. C **54**, 3043 (1996)
61. C.A. Bertulani, P. Danielewicz, Introduction to nuclear reactions (Institute of Physics Publishing, 2004)
62. http://www.nuclear.theory.net/NPE/Talentmaterial/index2.htlm
63. G.F. Bertsch, K. Henken, H. Esbensen, Nuclear breakup of Borromean nuclei. Phys. Rev. C **57**, 1366 (1998)
64. J. Tostevin, J. Al-Khalili, Sizes of the He isotopes deduced from proton elastic scattering measurements. Nucl. Phys. A **616**, 418c (1997)
65. J. Al-Khalili, J. Tostevin, I. Thompson, Radii of halo nuclei from cross section measurements. Phys. Rev. C **54**, 1843 (1996)
66. J. Tostevin et al., Single-neutron removal reactions from ^{15}C and ^{11}Be: deviations from the eikonal approximation. Phys. Rev. C **66**, 024607 (2002)
67. D. Bazin et al., Mechanisms in knockout reactions. Phys. Rev. Lett. **102**, 232501 (2009)
68. T. Aumann, Private communication (2013)
69. H. Grawe, Shell Model from a Practitioner's Point of View, in *The Euroschool Lectures on Physics with Exotic Beams*, vol. I (2004), pp. 33–76
70. T. Otsuka, Shell Structure of Exotic Nuclei, in *The Euroschool Lectures on Physics with Exotic Beams*, vol. III (2009), pp. 1–25
71. Shell model code ANTOINE, http://sbgat194.in2p3.fr/~theory/antoine/intro.html
72. Shell model code NuShell, http://www.garsington.eclipse.co.uk
73. Shell model OXBASH, http://arxiv.org/abs/nucl-th/9406020
74. R. Roth et al., Ab initio calculations of medium-mass nuclei with normal-ordered chiral $NN + 3N$ interactions. Phys. Rev. Lett. **109**, 052501 (2012)
75. G. Hagen et al., Continuum effects and three-nucleon forces in neutron-rich oxygen isotopes. Phys. Rev. Lett. **108**, 242501 (2012)
76. H. Hergert et al., Ab initio calculations of even oxygen isotopes with chiral two-plus-three-nucleon interactions. Phys. Rev. Lett. **110**, 242501 (2013)
77. Ch. Forssén et al., Systematics of 2^+ states in C isotopes from the ab initio no-core shell model. J. Phys. G, Nucl. Part. Phys. **40**, 055105 (2013)
78. V. Somà et al., Ab initio Gorkov-Green's function calculations of open-shell nuclei. Phys. Rev. C **87**, 011303(R) (2013)
79. http://www.fair-center.eu/
80. http://www.frib.msu.edu/
81. W. Mittig, Spectromètres magnetiques et electriques comme detecteurs de haute resolution et comme filtres selectifs. Ecole Joliot-Curie (1994)
82. D.J. Morrisey, B. Sherrill, *In-Flight Separation of Projectile Fragments*. Euroschool on Exotic Beams, vol. 1 (Springer, Berlin, 2004), ISBN 3-540-22255-3
83. H. Geissel et al., A versatile magnetic system for relativistic heavy ions. Nucl. Inst. Methods Phys. Res. B **70**, 286 (1992)
84. D.J. Morrissey et al., A new high-resolution separator for high intensity secondary beams. Nucl. Instrum. Methods Phys. Res. B **126**, 316 (1997)
85. D. Bianchi et al., SPEG: an energy loss spectrometer for GANIL. Nucl. Instr. Methods Phys. Res. A **276**, 509 (1989)

86. Th. Baumann, Longitudinal momentum distributions of ^{8}B and ^{19}C: signatures for one-proton and one-neutron halos. Ph.D. Dissertation, University of Giessen (1999)
87. http://lise.nscl.msu.edu/documentation.html
88. http://web-docs.gsi.de/~weick/mocadi/
89. J. Eberth et al., MINIBALL A Ge detector array for radioactive ion beam facilities. Prog. Part. Nucl. Phys. **46**, 389 (2001)
90. P. Maierbeck et al., Structure of ^{55}Ti from relativistic one-neutron knockout. Phys. Lett. B **675**, 22 (2009)
91. M. Honma et al., Effective interaction for pf-shell nuclei. Phys. Rev. C **65**, 061301 (2002)
92. Technical design report of the CALIFA Barrel Detector, http://www.fair-center.eu/en/for-users/publications/experiment-collaboration-publications.html
93. https://www.gsi.de/en/work/research/nustarenna/kernreaktionen/activities/r3b.htm
94. T. Nakamura et al., Observation of strong low-lying E1 strength in the two-neutron halo nucleus ^{11}Li. Phys. Rev. Lett. **96**, 252502 (2006)
95. H. Simon et al., Systematic investigation of the drip-line nuclei ^{11}Li and ^{14}Be and their unbound subsystems ^{10}Li and ^{13}Be. Nucl. Phys. A **791**, 267 (2007)
96. M. Zinser et al., Invariant-mass spectroscopy of ^{10}Li and ^{11}Li. Nucl. Phys. A **619**, 151 (1997)
97. M.S. Wallace et al., The high resolution array (HiRA) for rare isotope beam experiments. Nucl. Instrum. Methods Phys. Res. A **583**, 302 (2007)
98. C. Rodriguez, Ph.D. Thesis Universidad de Santiago de Compostela, http://www.usc.es/genp
99. B. Jonson, Light dripline nuclei. Phys. Rep. **289**, 1 (2004)
100. J. Al-Kahalili, An introduction to Halo Nuclei, in *The Euroschool Lectures on Physics with Exotic Beams*, vol. I (2004), pp. 77–112
101. K. Riisager, Nuclear Halos and experiment to probe them, in *The Euroschool Lectures on Physics with Exotic Beams*, vol. II (2006), pp. 1–36
102. D.J. Millener et al., Strong E1 transitions in ^{9}Be, ^{11}Be, and ^{13}C. Phys. Rev. C **28**, 497 (1983)
103. J.H. Kelley et al., Parallel momentum distributions as a probe of halo wave functions. Phys. Rev. Lett. **74**, 30 (1995)
104. F.M. Nunes, I.J. Thompson, R.C. Johnson, Core excitation in one neutron halo systems. Nucl. Phys. A **596**, 171 (1996)
105. T. Suzuki, T. Otsuka, A. Muta, Magnetic moment of ^{11}Be. Phys. Lett. B **364**, 69 (1995)
106. D.L. Auton, Direct reactions on ^{10}Be. Nucl. Phys. A **157**, 305 (1970)
107. B. Zwieglinski, W. Benenson, R.G.H. Robertson, Study of the ^{10}Be$(d,p)^{11}$Be reaction at 25 MeV. Nucl. Phys. A **315**, 124 (1979)
108. N.K. Timofeyuk, R.C. Johnson, Deuteron stripping and pick-up on halo nuclei. Phys. Rev. C **59**, 15 (1999)
109. R. Anne et al., Exclusive and restricted-inclusive reactions involving the ^{11}Be one-neutron halo. Nucl. Phys. A **575**, 125 (1994)
110. T. Nakamura et al., Exclusive and restricted-inclusive reactions involving the ^{11}Be one-neutron halo. Phys. Lett. B **331**, 296 (1994)
111. T. Aumann et al., One-neutron knockout from individual single-particle states of ^{11}Be. Phys. Rev. Lett. **84**, 35. 45 (2000)
112. E.K. Warburton, B.A. Brown, Effective interactions for the 0p1s0d nuclear shell-model space. Phys. Rev. C **46**, 923 (1992)
113. W. Schwab et al., Obsevation of a proton-halo in ^{8}B. Z. Phys. A **350**, 283 (1995)
114. M.H. Smedberg et al., New results on the halo structure of ^{8}B. Phys. Lett. B **452**, 1 (1999)
115. D. Cortina-Gil et al., One-nucleon removal cross-sections for ^{17,19}C and ^{8,10}B. Eur. Phys. J. A **10**, 49 (2001)
116. J.N. Bahcall et al., How uncertain are solar neutrino predictions? Phys. Lett. B **433**, 1 (1998)
117. Q.R. Ahmad et al., Measurement of the rate of $\nu_e + d \rightarrow p + p + e-$ interactions produced by ^{8}B solar neutrinos at the sudbury neutrino observatory. Phys. Rev. Lett. **87**, 071301 (2001)
118. M. Goeppert Mayer, *The Shell Model*. Nobel Lecture (1963)
119. J.H. Jensen, *Glimpses at the History of the Nuclear Structure Theory*. Nobel Lecture (1963)

120. R. Kanungo, A new view of nuclear shells. Phys. Scr. T **152**, 014002 (2013)
121. I. Tanihata, H. Savajols, R. Kanungo, Recent experimental progress in nuclear halo structure studies. Prog. Part. Nucl. Phys. **68**, 215 (2013)
122. T. Otsuka et al., Magic numbers in exotic nuclei and spin-isospin properties of the NN interaction. Phys. Rev. Lett. **87**, 082502 (2001)
123. T. Otsuka et al., Evolution of nuclear shells due to the tensor force. Phys. Rev. Lett. **95**, 232502 (2005)
124. T. Otsuka et al., Three-body forces and the limit of oxygen isotopes. Phys. Rev. Lett. **105**, 232501 (2010)
125. T. Otsuka, Exotic nuclei and nuclear forces. Phys. Scr. T **152**, 014007 (2013)
126. S.C. Pieper, R.B. Wiringa, J. Carlson, Quantum Monte Carlo calculations of excited states in $A = 6$–8 nuclei. Phys. Rev. C **70**, 054325 (2004)
127. J. Holt et al., Three-body forces and shell structure in calcium isotopes. J. Phys. G, Nucl. Part. Phys. **39**, 085111 (2012)
128. H. Simon et al., Direct experimental evidence for strong admixture of different parity states in ^{11}Li. Phys. Rev. Lett. **83**, 496 (1999)
129. I. Tanihata et al., Measurement of two-halo neutron transfer reaction $p(^{11}\mathrm{Li}, ^{9}\mathrm{Li})t$ at 3 A MeV. Phys. Rev. Lett. **100**, 192502 (2008)
130. S. Fortier et al., Core excitation in $^{11}\mathrm{Be}_{gs}$ via the $p(^{11}\mathrm{Be}, ^{10}\mathrm{Be})d$ reaction. Phys. Lett. B **461**, 22 (1999)
131. W. Geithner et al., Measurement of the Magnetic Moment of the One-Neutron Halo Nucleus ^{11}Be. Phys. Rev. Let. **83**, 3792 (1990)
132. J.R. Terry et al., Direct evidence for the onset of intruder configurations in neutron-rich Ne isotopes. Phys. Lett. B **640**, 86 (2006)
133. J.R. Terry et al., Single-neutron knockout from intermediate energy beams of ^{30,32}Mg: mapping the transition into the island of inversion. Phys. Rev. C **77**, 014316 (2008)
134. C.R. Hofman et al., Evidence for a doubly magic ^{24}O. Phys. Lett. B **672**, 17 (2009)
135. K. Tshoo et al., The $N = 16$ spherical shell closure in ^{24}O. http://arxiv.org/pdf/1205.5657.pdf
136. W.F. Mueller et al., Nucl. Instrum. Methods Phys. Res. A **466**, 492 (2001)
137. A. Obertelli et al., $N = 16$ subshell closure from stability to the neutron drip line. Phys. Rev. C **71**, 024304 (2005)
138. J. Tostevin, Core excitation in halo nucleus break-up. J. Phys. G **25**, 735 (1999)
139. M. Honma, T. Otsuka, B.A. Brown, T. Mizusaki, Shell model description of neutron-rich pf-shell nuclei with a new effective interaction GXPF1. Eur. Phys. J. A **25**, 499 (2005)
140. J. Tostevin, G. Podolyak, B.A. Brown, P.G. Hansen, Correlated two-nucleon stripping reactions. Phys. Rev. C **70**, 064602 (2004)
141. J.A. Tostevin, B.A. Brown, Diffraction dissociation contributions to two-nucleon knockout reactions and the suppression of shell-model strength. Phys. Rev. C **74**, 064604 (2006)
142. E.C. Simpson et al., Two-nucleon knockout spectroscopy at the limits of nuclear stability. Phys. Rev. Lett. **102**, 132502 (2009)
143. K. Wimmer et al., Probing elastic and inelastic breakup contributions to intermediate-energy two-proton removal reactions. Phys. Rev. C **85**, 051603(R) (2012)
144. E.C. Simpson, J.A. Tostevin, One-and two-neutron removal from the neutron-rich carbon isotopes. Phys. Rev. C **79**, 024616 (2009)
145. http://www.gsi.de/work/forschung/nustarenna/kernreaktionen/activities/elise.htm
146. A. Gade et al., Reduced occupancy of the deeply bound $0d5 = 2$ neutron state in ^{32}Ar. Phys. Rev. Lett. **93**, 042501 (2004)
147. A. Gade et al., Reduction of spectroscopic strength: weakly-bound and strongly-bound single-particle states studied using one-nucleon knockout reactions. Phys. Rev. C **77**, 044306 (2008)
148. W.H. Dickhoff, C. Barbieri, Self-consistent Green's function method for nuclei and nuclear matter. Prog. Part. Nucl. Phys. **52**, 377 (2004)
149. T. Kobayashi et al., $(p, 2p)$ reactions on $^{9-16}$C at 250 MeV/A. Nucl. Phys. A **805**, 431 (2008)

150. N.S. Chant, P.G. Roos, Distorted-wave impulse-approximation calculations for quasifree cluster knockout reactions. Phys. Rev. C **15**, 57 (1977)
151. N.S. Chant, P.G. Roos, Spin orbit effects in quasifree knockout reactions. Phys. Rev. C **27**, 1060 (1983)
152. T. Aumann, C.A. Bertulani, J. Ryckebusch, Quasi-free $(p, 2p)$ and (p, pn) reactions with unstable nuclei, to be published. arXiv:1311.6734v1 [nucl-theo]
153. N. Austern et al., Continuum-discretized coupled-channels calculations for three-body models of deuteron-nucleus reactions. Phys. Rep. **154**, 125 (1987)
154. F. Nunes, Continuum-discretised coupled channels methods, http://www.scholarpedia.org/article/Continuum-Discretised-Coupled-Channels-methods
155. A. Moro, F. Nunes, Transfer to the continuum and breakup reactions. Nucl. Phys. A **767**, 138 (2006)
156. E. Alt et al., Reduction of the three-particle collision problem to multi-channel two-particle Lippmann-Schwinger equations. Nucl. Phys. B **2**, 167 (1967)
157. R. Crespo et al., Spectroscopy of unbound states under quasifree scattering conditions: one-neutron knockout reaction of ^{14}Be. Phys. Rev. C **79**, 014609 (2009)
158. H. Geissel et al., The super-FRS project at GSI. Nucl. Instrum. Methods Phys. Res. B **204**, 71 (2003)
159. J.T. Taylor, Proton induced quasi-free scattering with inverse kinematics. Ph.D. Thesis, University of Liverpool (2011)
160. V. Panin, Fully exclusive measurements of quasi-free single-nucleon knockout reactions in inverse kinematics. Ph.D. Thesis Technical, University of Darmstadt (2012)
161. www-aladin.gsi.de/www/kp3/aladinhome.html
162. T. Blaich et al., A large area detector for high-energy neutrons. Nucl. Instr. Methods Phys. Res. A **314**, 132 (1992)
163. Ch. Caesar et al., Beyond the neutron drip line: the unbound oxygen isotopes ^{25}O and ^{26}O. Phys. Rev. C **88**, 034313 (2013)
164. O. Tengblad et al., $LaBr_3$(Ce):$LaCl_3$(Ce) phoswich with pulse shape analysis for high energy gamma-ray and proton identification. Nucl. Instrum. Methods Phys. Res. A **704**, 19 (2013)
165. A. Obertelli, *Magic numbers off stability*, ERC Starting Grant (2010–2015) 258567